High Temperature Integrated Thermoelectric System and Materials

Final Scientific/Technical Report

Reporting Period: July 1, 2010 to March 31, 2011

Principal Author(s): Mike S. H. Chu

Report Issuing Date: June 7, 2011

DOE Award Number: DE-SC0004299

Report Submitting Organization:

TAM Ceramics, LLC

4511 Hyde Park Blvd.

Niagara Falls, NY 14305, USA

Phone: 716-278-9423

FAX: 716-285-3026

E-Mail: mchu@tamceramics.net

TABLE OF CONTENTS page

1.0 ABSTRACT

The final goal of this project is to produce, by the end of Phase II, an all ceramic high temperature thermoelectric module. Such a module design integrates oxide ceramic n-type, oxide ceramic p-type materials as thermoelectric legs and oxide ceramic conductive material as metalizing connection between n-type and p-type legs. The benefits of this all ceramic module are that it can function at higher temperatures (> 700°C), it is mechanically and functionally more reliable and it can be scaled up to production at lower cost. With this all ceramic module, millions of dollars in savings or in new opportunities recovering waste heat from high temperature processes could be made available. A very attractive application will be to convert exhaust heat from a vehicle to reusable electric energy by a thermoelectric generator (TEG).

Phase I activities were focused on evaluating potential n-type and p-type oxide compositions as the thermoelectric legs. More than 40 oxide ceramic powder compositions were made and studied in the laboratory. The compositions were divided into 6 groups representing different material systems. Basic ceramic properties and thermoelectric properties of discs sintered from these powders were measured. Powders with different particles sizes were made to evaluate the effects of particle size reduction on thermoelectric properties. Several powders were submitted to a leading thermoelectric company for complete thermoelectric evaluation.

Initial evaluation showed that when samples were sintered by conventional method, they had reasonable values of Seebeck coefficient but very low values of electrical conductivity. Therefore, their power factors (PF) and figure of merits (ZT) were too low to be useful for high temperature thermoelectric applications. An unconventional sintering method, Spark Plasma Sintering (SPS) was determined to produce better thermoelectric properties. Particle size reduction of powders also was found to have some positive benefits.

Two composition systems, specifically 1.0 SrO – 0.8x1.03 TiO2 – 0.2x1.03 NbO2.5 and 0.97 TiO2 – 0.03 NbO2.5, have been identified as good base line compositions for n-type thermoelectric compositions in future module design. Tests of these materials at an outside company were promising using that company's processing and material expertise. There was no unique p-type thermoelectric compositions identified in phase I work other than several current cobaltite materials. Ca3Co4O9 will be the primary p-type material for the future module design until alternative materials are developed.

BaTiO3 and rare earth titanate based dielectric compositions show both p-type and n-type behavior even though their electrical conductivities were very low. Further research and development of these materials for thermoelectric applications is planned in the future.

A preliminary modeling and optimization of a thermoelectric generator (TEG) that uses the n-type 1.0 SrO – 1.03x0.8 TiO2 – 1.03x0.2 NbO2.5 was performed.

Future work will combine development of ceramic powders and manufacturing expertise at TAM, development of SPS at TAM or a partner organization, and thermoelectric material/module testing, modeling, optimization, production at several partner organizations.

2.0 EXECUTIVE SUMMARY

The final goal of this project is to produce, by the end of Phase II, an all ceramic high temperature thermoelectric module. Such a module consists of oxide ceramic n-type, oxide ceramic p-type materials as thermoelectric legs and oxide ceramic conductive material as metalizing connection between n-type and p-type legs. Because of all ceramic components, the module should have advantages of (a) It can operate at high temperatures above 700°C and up to 1000°C. Therefore, higher temperature difference can be established to have higher energy conversion efficiency, (b) It can extend the application to some industrial processes that no current thermoelectric device is applicable, (c) It has better thermal matching among components and therefore can sustain more operating cycles, (d) It is less complicated and more cost effective to co-process all components together to make modules, and (e) It is cost effective to scale up the ceramic powder components, processes and the facilities are readily established. The overall effect is a thermoelectric module that is operable at higher temperatures, has higher conversion efficiency, has higher reliability and costs less to produce. With this all ceramic module, millions of dollars in savings or in new opportunities recovering waste heat from high temperature processes could be made available. A very attractive application will be to convert exhaust heat from a vehicle to reusable electric energy by a thermoelectric generator (TEG).

Phase I research work was focused mainly on studying the potential of several ceramic oxide formulations for high Seebeck coefficient, high electrical conductivity, and low thermal conductivity so to yield high power factor and high ZT suitable for thermoelectric application at high temperatures. A modeling and optimization of a thermoelectric module was then performed using thermoelectric properties of selected components.

Following the work plan, more than 40 ceramic powder compositions were made and tested in the laboratory. The compositions were divided into 6 groups representing different material systems. After the powders were made, ceramic disc samples were pressed and sintered either in air or in a reducing atmosphere (established by hydrogen/argon (H2/Ar) gas mixture). Basic ceramic properties and thermoelectric properties of sintered discs were then measured. Powders with different particles sizes were also made to evaluate the effects of particle size reduction on thermoelectric properties. Several powders were also submitted to a leading thermoelectric company for complete thermoelectric evaluation.

Initial evaluation showed that when samples were sintered by conventional method, they had reasonable values of Seebeck coefficients but very low values of electrical conductivities. Therefore, their power factors (PF) and figure of merits (ZT) were too low for high temperature thermoelectric applications. It was found that samples sintered by an unconventional method, Spark Plasma Sintering (SPS) technique, produced better thermoelectric properties. The improvement is mainly through improvement of electrical conductivity. It is believed now that SPS is a key processing step to produce high temperature oxide thermoelectric materials.

Particle size reduction of the ceramic thermoelectric composition has benefits. It will be investigated and developed further.

Two composition systems, one based on doped TiO2 and one based on doped SrTiO3, have been identified as good precursor compositions for n-type thermoelectric compositions. Works were done specifically on 0.97 TiO2 – 0.03 NbO2.5, and 1.0 SrO – 0.8x1.03 TiO2 – 0.2x1.03 NbO2.5

compositions. Results at an outside company were promising using that company's processing and material expertise. With some process and/or material modification, ZT close to 0.25 was obtained. The goal in the future is to increase ZT to > 0.5.

An innovative approach was taken in formulation research. Nine $BaTiO_3$ or rare earth titanate based commercial dielectric compositions were evaluated for their thermoelectric properties. Several of them show potential as either n-type or p-type materials. They have high Seebeck coefficients in some cases near +/- 1000 μV/K even though their electrical conductivities are too low. Further development may be worthwhile. Again, key approach will be to increase their electrical conductivities through composition chemistry or through processing technique without giving away their Seebeck coefficients.

There are no unique p-type thermoelectric compositions identified in phase I work other than several current cobaltite materials that were reported in literature. $Ca_3Co_4O_9$ is the most available high temperature p-type material at this moment. Development of other p-type materials must continue in the future.

A preliminary modeling and optimization of a thermoelectric generator (TEG) that used the n-type 1.0 SrO – 1.03x0.8 TiO_2 – 1.03x0.2 $NbO_{2.5}$ was performed. This modeling and optimization technique is a very useful tool in estimating; (a) how practical physically, technically, and economically to fit chosen thermoelectric materials into an actual module to generate renewed usable energy, (b) optimum design of the TEG device, (c) material consumption of the TEG device, and (d) material and manufacturing cost of the TEG device.

Future works in are;

(1) Optimize (a) the SrO – TiO_2 – $NbO_{2.5}$, (b) TiO_2 – $NbO_{2.5}$ (or $TaO_{2.5}$), and (c) the dielectric composition systems to improve their thermoelectric properties. Target is to increase ZTs from current value (0.1 - 0.2) to 0.5 or above. Specific technical approaches will be to (a) develop an optimum formulation chemistry (dopant level, dopant type, stoichiometry), (b) develop particle size reduction technology and (c) develop and qualify raw material sources for scale up.

(2) Develop and optimize a non cobalite based p-type formulation. $SrTiO_3$ with p-type dopants and dielectric compositions are to be investigated as starting points. Technical approaches will be the same as proposed above for n-type materials.

(3) Develop and identify an oxide ceramic conductive metallization material. La_2O_3 – MnO_2 based compositions will be a starting point.

(4) Develop and optimize the SPS process to sinter individual component and module assembly.

(5) Develop a process to integrate p-type and n-type thermoelectric legs with metallization to build a prototype module device.

(6) Build prototype of the module. Test and verify against design outputs from modeling and optimization.

3.0 INTRODUCTION

3.1 Goals

The goal of DE-SC0004299 project was to study the feasibility of an all ceramic thermoelectric module. Such a module consists of oxide ceramic n-type, oxide ceramic p-type materials as thermoelectric legs and oxide ceramic conductive material as metalizing connection between n-type and p-type legs.

There are a number of advantages of the all ceramic module approach. Among them are:

Operating temperature range -- The module can operate at high temperatures above 700°C and up to 1000°C. It can extend its application to some industrial processes that no current thermoelectric device is applicable. Energy recovery from automobile exhaust would be an example.

Reliability-- It has better thermal matching among components and therefore can sustain more operating cycles.

Cost -- It is less complicated and more cost effective to co-process all components together to make the module.

Scale up -- It is cost effective. Industrial processes are readily established to scale up the ceramic components.

The overall effect is a thermoelectric module that can operate at high temperatures, has more energy conversion efficiency, has higher reliability and costs less to produce in large quantities.

3.2 Background

Industrial waste heat refers to energy that is generated in industrial processes without being recovered to practical use. There is a problem of inefficiency in today's industrial processes. Energy efficiency is important in vehicles, electric power stations, military machinery, and many industrial systems. Efficient use of energy can extend the operating lifetime of systems, extend mileage ranges, and enable more affordable operation. With the increasing cost of fossil fuels, improved efficiencies can result in substantial cost savings. Current commercially available thermoelectric conversion systems and materials can only function at waste heat temperatures below 500°C. This limitation leaves out many industrial processes where waste heats are generated at much higher temperatures. The limitation is due largely to a) no suitable low cost, higher temperature thermoelectric materials, b) mechanical failure caused by thermal expansion mismatch between thermoelectric components and conductive or metalized materials, c) design limitation in heat management, and d) other factors such as the costs of raw materials, processing, and manufacturing.

Early Thermoelectric (TE) materials research in the 1950s and 1960s yielded bismuth telluride (Bi_2Te_3), lead telluride (PbTe) and silicon-germanium (SiGe) alloys as the materials with the best figure of merits in three somewhat distinct temperature ranges. Bi_2Te_3 and its alloys have been used extensively in TE refrigeration applications, some niche low power generation applications, and have a useful temperature range of 180°K to 450°K. PbTe and SiGe materials have been used extensively in higher temperature power generation applications, particularly spacecraft power generation, and have a useful temperature range of 500°K to 900°K

and 800°K to 1300°K, respectively [1]. The discovery of these materials as good candidates for TE devices led to continuous and numerous research and development of TE materials with high energy conversion efficiency. The energy conversion efficiency of TE material is gauged by a parameter called Figure of Merit, ZT. ZT is dimensionless and is defined as;

$$ZT = (Q^2 \times \sigma \times T)/k, \quad (1)$$

where Q (μV/°K) is the Seebeck coefficient of the material, σ (S/cm) is the electrical conductivity of the material, T (K) is the absolute temperature and k (watt/m-K) is the thermal conductivity of the material.

However, much less amount of work were devoted to show how these materials could be integrated into a device module and how the device module will function effectively with high efficiency. Thermoelectric device efficiency is defined as;

$$\eta_{\max} = \left[\frac{T_h - T_c}{T_h}\right] \cdot \left[\frac{\left(1 + Z^*\overline{T}\right)^{1/2} - 1}{\left(1 + Z^*\overline{T}\right)^{1/2} + 1}\right], \quad (2)$$

where,

Z^* is the optimum Z of the p-type/n-type couple in the TE device,
T_h and T_c are the temperatures of the hot and the cool sides respectively, and
$\overline{T}$ is the average of T_h and T_c.

As can be seen from the equation above, device efficiency is not only dependant on ZT, which is only part of the equation, temperature difference between the hot and cold side is equally important. For that reason having a high thermal resistance in the material is important to hold as high a temperature difference as possible. The above argument is basically saying that TE technology development consists of two important parts. That is; material development to achieve high ZT and thermal management to operate with high temperature hot side and to sustain high temperature difference between hot side and cold side.

Cost effectiveness is another important but sometimes forgotten factor. The TE device has to be cost effective to produce commercially to find its acceptance to the end user. A good parameter to judge is the dollar per watt number. That is how much the device will cost the user to purchase vs. how much power the device can deliver. Among many other factors, the dollar per watt figure is impacted by raw materials cost, environmental impact, design costs, and manufacturing costs.

Currently SiGe is the best available TE material for high temperature uses, but costs of production have limited its uses to NASA applications in space. Although the SiGe materials can operate effectively in higher temperatures, there is no current module that can cost effectively match those temperatures. In order for the module to function at those higher temperatures, precious metals with high conductivity and very high melting points must be used such as platinum. These materials are not cost competitive with high temperature alternatives in many industries, such as bottom cycling. Thus in order to gain global adoption, a novel approach must be taken in module design. For many industries such as glass or metal smelting, the entire module, especially on the hot side, must be able to tolerate extreme temperatures for up to 10 years. Otherwise industrial corporations will be hesitant to purchase and install them in their

factories. Ceramics' main advantage in industry is its robust and durable nature in high temperature environments. Kilns, furnaces, and other such equipment are often made out of ceramics. Thus if the entire TE device is made out of ceramics, including the n-type, p-type, conductive contacts, and hot side heat exchanger then the entire device can operate at these high temperatures, and survive the industry required 10+ years of required operation.

3.3 Solution and Opportunity

The all ceramic TE technology allows for the opportunity to recapture the wasted energy generated at high temperatures up to and above 1000°C. The integrated thermoelectric system and materials can harvest those high temperature waste heat energies and convert them into electricity. Thermoelectric heat recovery technologies can frequently reduce the operating costs for facilities by increasing their energy productivity and energy efficiency. In Automobile industry, waste heat recovery from diesel or gasoline engine exhaust has the great benefits of increasing fuel efficiency, reducing carbon deposit, reducing weight, and reducing manufacturing cost of both military and commercial vehicles. In an extreme case, jet based aircraft have a huge available temperature difference between the jet exhaust and the passing air. The greater the temperature difference between the two sides of the thermoelectric materials, the more electricity can be harvested. The problem with current thermoelectric materials is they have not been able to operate above 300°C efficiently [2-4]. Either the material or the system, begins to breakdown under this heat. Thus current technologies have been unable to capture energy where most of it is available in the 700-1000°C range. The novel system developed under this project is all ceramic based and thus after development will be the first materials that can operate efficiently in that temperature range.

The market also demands a low cost of production as well as flexibility in uses. The technologic solution must be adaptable to harvesting heat in different applications ranging from power production plants to smaller vehicle power trains. The current commercially available state of the art in thermoelectric materials can only be used in temperatures below 500°C. Above that temperature it can no longer function as a result of the materials or modules losing stability. This prevents efficient use of thermoelectrics in recovering, for example, a vehicle's engine exhaust heat since half of the exhaust manifold is operated at peak temperatures between 600°C to 800°C. Another example is in a coal power plant, where the furnace heats water to 370°C in order to make steam, however to increase energy output the steam is superheated above 540°C. There are many industrial processes that generate waste heat above 800°C. In order to integrate thermoelectric waste heat recovery in power plants, these systems and materials will have to be resistant to much higher temperatures.

The all ceramic technology innovation is a novel system approach that integrates high temperature ceramic oxide thermoelectric materials, ceramic conductive oxide materials, and efficient module design that will be able to function at extreme temperatures (up to 1000°C). Thus it is far more energy efficient and can harvest thermal waste energy at temperatures current materials cannot tolerate. It can also be produced in a low cost manner, and form fitted to different industrial applications.

As a result we can meet military and commercial needs as well as overcoming technical obstacles. There is over $300 million in commercial potential in high heat industrial processes.[1] This market would be easier to integrate into than a space confined application

such as in vehicles. The all ceramic materials and technology can meet the specific energy and temperature requirements of operation where +1000°C waste heat is generated. After proof of principle we will have prototype testing with global partners in industrial settings. We can then continue to increase the sophistication for industrial applications such as steel mills and coal power plants, where temperatures are even higher

3.4 Anticipated Public Benefits

The application that would be most visible to the public would be to increase energy efficiency in combustion engine based transport. There by reducing America's carbon footprint, as well as dependency on foreign oil imports. Converting waste heat produced by motors into electricity would make cars far more efficient. There is an untapped opportunity that exists to harvest energy from the engine and exhaust infrastructure. According to BMW, automobiles are an example of high energy usage with low efficiency. Roughly 75% of the energy produced during peak combustion is lost in the exhaust and engine coolant in the form of heat. Already BMW states that fuel efficiency is increased by 12% with early thermoelectric prototypes. With DOE funding BSST, BMW, and Ford are working on these prototypes for passenger cars. If successful they would no longer need an alternator to recharge the car's battery, in both hybrid and non-hybrid models. Fuel efficiency, weight, air pollution, and the cost of the car can therefore be reduced.

As stated above, the breakdown of current thermoelectric energy conversion at high temperatures is not only due to thermoelectric materials but it could also be due largely to breakdown as caused by thermal expansion mismatch between thermoelectric materials and, for example, metallization components. This is why it is important to have high temperature strength in these materials. The current system could barely create enough energy for standard car batteries, while with the all ceramic integrated system it could function satisfactory in much higher temperatures up to 1000°C. As a result the reliability and fuel efficiency can be improved, while weight and costs can be reduced.

If this all ceramic technology is broadly adopted, we expect that in automobile industry alone, it could reduce fuel consumption by American drivers by over 10% resulting in savings of as many as 2,068,000 barrels of crude per day according to the CIA World Factbook. American drivers would save at least 10% of the money they spend on fuel as well as reducing the cost of buying and maintaining a car. The initial expectations are that the system would cost only 50% of the cost of an alternator, and would have a much longer lifetime and less maintenance problems. The cost savings when the all ceramics technology is applied to other industrial processes such as coal power plant, jet combustion engine could be equally as large and significant. Table 1 below shows a breakdown of the potential waste heat by industry and is from the 2006 DOE Engineering Scoping Study of Thermoelectrics.

These industries could provide additional electricity either within their factories or to the grid that would not add any emissions or require any additional fuel sources. This could lower emissions per kilo-watt-hour (kwh) for those factories, reduce emissions per unit of production, and lastly save the industries on their electric expenses. This effect could be seen through American and Global industries and could be an important tool for meeting Cap and Trade and global emission goals in the future.

3.5 Technical Approaches and Schedule

Major technical approach in Phase I was focused on increasing conductivities of several baseline ceramic oxide composition systems without affecting their Seebeck coefficients by i) stoichiometry variation, ii) donor (n-type) / acceptor (p-type) doping and iii) processing conditions (sintering technique, sintering temperature, sintering atmosphere, milling, etc.). At the end of Phase I the approach was to design an integrated thermoelectric energy conversion module that uses high temperature oxide ceramic thermoelectric materials, high temperature oxide conductive metallization and high temperature ceramic isolating materials. The design and evaluation of the integrated TE module will be performed at Clarkson University using mathematical models describing: convective and conductive heat transfer, fluid flow, and thermoelectric power conversion.

Table 1: Thermoelectric waste heat opportunities in the U.S. industries

		Temperature C (°F)	Available Waste Heat *TBtu/year*	TEG Recoverable Waste Heat *TBtu/year*		
				ZT=1	*ZT=2*	*ZT= 4*
Applications Set A: (low hot-side temperature, relatively clean flue gas)						
Commercial	Water/Steam Boilers	150°C (300°F)	560	na	na	na
Industrial	Water/Steam Boilers[5]	150°C (300°F)	610	na	na	na
	Ethylene Furnace	150°C (300°F)	30	na	na	na
Applications Set B: (medium hot-side temperature, mixed flue gas quality)						
	Aluminum Smelting[6]	960°C (1750°F)	4.2	0.2	0.6	1.0
	Aluminum Melting[7]	750°C (1380°F)	28.6	1.4	4.3	7.2
	Metal Casting Iron Cupola	375°C (700°F)				
	Steel Blast Furnace					
	Lime Kiln					
	Cement Kiln (with preheater)	200°C (380°F)	7.0	0.3	1.0	1.7
Applications Set C: (high hot-side temperature, mixed flue gas quality)						
	Cement Kiln (no preheat)	820°C (1500°F)	8.4	0.4	1.3	2.1
	Glass oxy-fuel Furnace	1425°C(2600°F)	4.8	0.2	0.7	1.2
	Glass Regenerative Furnace	480°C (900°F)	11.8	0.6	1.8	3.0
		Total	**1,265**	**3.2**	**9.7**	**16.2**

This modeling and optimization technique is a very useful tool in estimating; (a) how practical physically, technically, and economically to fit chosen thermoelectric materials into an actual module to generate renewed usable energy, (b) optimum design of the TEG device, (c) material consumption of the TEG device, and (d) material and manufacturing cost of the TEG device.

Table 2 is a Phase I work plan.

Task Names \ Month	1	2	3	4	5	6	7	8	9
Task 1 Prepare Samples									
Task 2 Thermoelectric Measurement									
Task 3 Characterization of powders and ceramics									
Task 4 Composition and Process Modification									
Task 5 Design of Commercial Prototype									
Task 6 Final Report									

Table 2 Phase I Work Plan

4.0 Technical Approaches

4.1 Task 1 and Task 2, Prepare Samples and Thermoelectric Measurement

4.1.1 Powder Synthesis

More than 40 ceramic oxide compositions for preliminary study were prepared by conventional oxide reaction route. Table 3 is a list of powder compositions made. As indicated in Table 3, the compositions were divided into 6 groups. Reasons why these compositions were selected are briefly explained.

Group 1: Doped TiO2 (Samples 001-006, 039, 015-017, and 019-021). These compositions were selected for study based on an early work done at TAM Ceramics in 1960s [5]. The expectations were that Nb2O5 and Ta2O5 doped compositions will exhibit n-type thermoelectric behavior and CuO and Li2O doped compositions will exhibit p-type thermoelectric behavior.

Group 2: Doped CeO2 (Samples 007-009, 044, 012-014). These compositions were selected also based on the early work done at TAM Ceramics in 1960s. The expectations were that Nb2O5 doped compositions will exhibit n-type thermoelectric behavior and CuO doped compositions will exhibit p-type behavior.

Group 3: SrTiO3 or Doped SrTiO3 (Samples 010-011 and 040). These were selected based on recommendations from several material experts and literatures [6-10]. The expectation was that they will exhibit n-type behavior.

Group 4: Mn and Co based (Samples 018 and 022-028). Mn based compositions are shown in literature [11-15] to have n-type behavior and Co based compositions are shown in the literature to have p-type behavior [16-20]. Literature reports tend to suggest it might be possible to sinter these Mn and Co based compositions in air to yield high electrical conductivities to give high ZTs for high temperature thermoelectric application. Sintering ceramics in air is the most economic approach for production.

Group 5: Co, Fe, Ni titanate based (Samples 041-043). These compositions were recommended by material experts [21-22]. Whether these compositions exhibit p-type or n-type thermoelectric behavior was a subject of this study.

Sample Number	Composition	Group	Target (N or P Type)
001	0.8 TiO2 - 0.2 TaO2.5	1	N
002	0.6 TiO2 - 0.4 TaO2.5	1	N
003	0.4 TiO2 - 0.6 TaO2.5	1	N
004	0.8 TiO2 - 0.2 NbO2.5	1	N
005	0.6 TiO2 - 0.4 NbO2.5	1	N
006	0.4 TiO2 - 0.6 NbO2.5	1	N
039	0.97 TiO2 - 0.03 NbO2.5	1	N
015	0.98 TiO2 - 0.02 CuO	1	P
016	0.96 TiO2 - 0.04 CuO	1	P
017	0.94 TiO2 - 0.06 CuO	1	P
019	0.98 TiO2 - 0.02 LiO0.5	1	P
020	0.95 TiO2 - 0.05 LiO0.5	1	P
021	0.92 TiO2 - 0.08 LiO0.5	1	P
007	0.98 CeO2 - 0.02 NbO2.5	2	N
008	0.96 CeO2 - 0.04 NbO2.5	2	N
009	0.94 CeO2 - 0.06 NbO2.5	2	N
044	0.874 CeO2 - 0.126 NbO2.5	2	N
012	0.98 CeO2 - 0.02 CuO	2	P
013	0.96 CeO2 - 0.04 CuO	2	P
014	0.94 CeO2 - 0.06 CuO	2	P
010	3 SrO - TiO2 - NbO2.5	3	N
011	3 SrO - TiO2 - TaO2.5	3	N
040	SrO - 0.8 TiO2 - 0.2 NbO2.5	3	N
018	0.5 BaO - 0.5 SrO - 0.6 CoO - 0.4 FeO1.5	4	P
022	CaMnO3	4	N
023	CaMnO3 - BaTiO3 - Nb2O5 - CoO	4	N
024	CaMnO3 - CeO2 - Nb2O5	4	N
025	CaMnO3 - TiO2 - Nb2O5	4	N
026	CaMnO3 - BaTiO3	4	N
027	Ca3Co4O9	4	P
028	CaCo(3)Ti(4)O12	4	P
041	SrO - 0.6 CoO - 0.4 FeO1.5	5	P
042	0.2 SrO - 0.4 NiO - 0.4 FeO1.5 - TiO2	5	P
043	0.2 CaO - 0.4 NiO - 0.4 FeO1.5 - TiO2	5	P
029	X7R302H	6	N or P
030	NPO610H	6	N or P
031	COG600H	6	N or P
032	COG350H	6	N or P
033	BaTiO3	6	N or P
034	COG630L	6	N or P
035	Y5V163L	6	N or P
036	Z5U113H	6	N or P
037	X7R302H - Ba(0.5)Sr(0.5)Co(0.6)Fe(0.4)O3	6	N or P

Table 3 List of Compositions Studied

Group 6: Dielectric Materials (Samples 029-037). These compositions were not included in the original study plan of this DOE proposal. The idea came after the grant was rewarded. It involved evaluating several commercially available dielectric powder formulations that had been manufactured in the past by TAM Ceramics and had been used by TAM's customers to manufacture multilayer ceramic capacitors or microwave resonators. The reasons for studying thermoelectric properties of these materials are i) It is an innovative approach since dielectric materials has not been studied for thermoelectric applications, ii) Sintered grain size of these materials are small due to they are for thin layer multilayer capacitor applications, iii) Even though the conductivity of these materials, as they are currently formulated for dielectric applications, should be very low, it was felt that it might be feasible to improve their conductivities by sintering or composition modification and iv) TAM has facilities and long time experience in manufacturing these powder formulations commercially. Therefore, if good thermoelectric applicable materials can be developed from these dielectric materials, they can readily be scaled up to manufacturing at TAM Ceramics.

In the original proposal, 8 compositions containing potassium were proposed. After preliminary laboratory work, it was found that when potassium carbonate (K_2CO_3) was used as raw material source, it was very difficult to mix with other oxide and/or carbonate components in water. The slurry was very thick and remained wet even after long period of time in the drying oven. Also, apparently because of the poor mixing and much lower melting point of K_2CO_3, calcine was not possible. The mixture turned into a melted mass even at low calcine temperatures. It was obvious these powders cannot be synthesized by the conventional oxide reaction route as outlined in Task 1 and Task 2 plans. For these powders, development works such as mixing technique and potassium raw material source needs to be developed beforehand. It was then decided to skip these potassium containing compositions in order to focus on evaluation of the other material systems.

It was planned in the original proposal to make several powder compositions at Alfred University by Pechini or chemical precipitation method to compare with powders made by solid state reaction method. Upon further review of the plan, this work seems to be of academic interests only since it is well accepted that powders synthesized by Pechini method or by chemical precipitation method will cost more and will be difficult to scale up to commercial quantity. Plus, as reported later a composition that is suitable for comparing different synthesis routes was identified only very recently. Therefore, such work will be deferred to a later time.

Table 4 is a list of raw material sources that had been used for making the compositions

For each composition, 50 to 70 grams total of raw materials of carbonates or oxides were weighed according to the composition together with Darvan "C" (R.T. Vanderbilt, Norwalk, CT) dispersant (1 wt % of total solids), deionized water (100 wt% of total solids), and two glass mixing balls in a small plastic bottle. Weighting was to within +/- 10 mg. The plastic bottle was then sealed and placed in a Spex paint mixer and vibratory mixed for 10 minutes. The wet slurry was discharged into a glass drying pan and oven dried at about 250°F overnight. If more than 100 grams of powder batch was to be made, multiple 50 to 70 gram batches were Spex mixed according to the above procedure and then each bottle of slurry was discharged into same glass drying pan to combine them into a single larger batch. The dried powder cake was then broken up with a mortar and pestle and screened through a 40 mesh nylon screen. The screened powder mix was then loaded into several zirconia saggers and calcined in a batch kiln with $MoSi_2$ heating elements (Model 305 Cladan Technology, Inc. San Marcos, CA) at temperatures of 1050°C or 1150°C in air for 4 hours. Weight of powder mix before and after calcine was recorded and the % weight loss (LOI) of the powder mix after calcine was calculated and compared with the theoretical LOI value to ensure all the carbonates were converted into oxides. The calcined powder was then ball milled in deionized water with 0.2 inch diameter yttria stabilized zirconia media for 10 to 24 hours. After milling, the slurry was dried and powder was again broken up by a mortar and pestle and screened through a 40 mesh screen and collected for future use. Most of the composition powders thus prepared had average powder particle size of 0.7 to 1.5 micron, measured by Microtrac-X100 particle size analyzer (HoneyWell, Clearwater, FL). Several CuO and Li_2O doped powders had bi-modal particle size distribution with coarse particle size portion of 5 to 7 microns. Particle sizes of Co, Mn, and Fe based powders were not measured due to lack of developed measurement procedure. The dielectric materials (Samples 29 – 38) were chosen from standard production lot without further processing. Their powder particle sizes are from 0.7 to 1.5 micron.

Raw Material	Source	Purity
BaCO3	NOAH Technologies, Code 11125 San Antonio, TX	99%
BaTiO3	TAM Ceramics, HPB Niagara Falls, NY	99.5%
CaCO3	NOAH Technologies, Code 11688 San Antonio, TX	99%
	Solvay, CF800 Houston, TX	99.5%
	Alfa Aesar, Stock 11403 Ward Hill, MA	99.5%
CeO2	NOAH Technologies, Code 18421 San Antonio, TX	99.9%
CoO	NOAH Technologies, Code 18382 San Antonio, TX	99.5%
	Shepherd, #1485W Norwood, OH	95.0%
CuO	NOAH Technologies, Code 12569 San Antonio, TX	99+%
Fe2O3	Alfa Aesar, Stock 12375 Ward Hill, MA	99.5%
Li2CO3	Alfa Aesar, Stock 36225 Ward Hill, MA	99+%
MnCO3	NOAH Technologies, Code 13603 San Antonio, TX	99.95%
	Alfa Aesar, Stock 14344 Ward Hill, MA	99.9%
	TAM Ceramics, E4203 Niagara Falls, NY	95.0%
Nb2O5	NOAH Technologies, Code 14937 San Antonio, TX	99.8%
	TAM Ceramics, E4225 Niagara Falls, NY	99.8%
NiO	NOAH Technologies, Code 16569 San Antonio, TX	99%
SrCO3	NOAH Technologies, Code 18297 San Antonio, TX	99.5%
	Alfa Aesar, Stock 14343 Ward Hill, MA	99%
	Solvay, HPL300 Houston, TX	99.8%
TiO2	NOAH Technologies, Code 90480 San Antonio, TX	99.9%
	Kronos, Grade 1000 Quebec, Canada	99%
Ta2O5	NOAH Technologies, Code 14937 San Antonio, TX	99.9%
X7R302H	TAM Ceramics Dielectric Product	Composite
NPO610H	TAM Ceramics Dielectric Product	Composite
COG600H	TAM Ceramics Dielectric Product	Composite
COG350H	TAM Ceramics Dielectric Product	Composite
COG630L	TAM Ceramics Dielectric Product	Composite
Y5V163L	TAM Ceramics Dielectric Product	Composite
Z5U113H	TAM Ceramics Dielectric Product	Composite

Table 4 List of Raw Material Sources

In order to maximize the number of compositions to be surveyed within the project time period, a fixed calcine temperature of either 1050°C or 1150°C, was selected to calcine the powder mixes. These two temperatures for calcining the powder mixes were selected based on TAM

Ceramics previous experience synthesizing powders of similar compositions. Study of phase formation utilizing DTA, TGA, XRD etc. will be a significant part of process engineering activities to improve powder performance at the commercialization stage.

4.1.2 Disc Preparation and Sintering

For sintering in air, the milled powder was added with 8 to 10 wt% of a binder solution made from corn syrup (Karo Light Corn Syrup, food store shelf item, ACH Food Company) diluted with equal amount of deionized water. The powder and binder were hand mixed thoroughly with a mortar and pestle, and screened through a 40 mesh nylon screen. 0.8 to 1.2 grams of powder was then loaded into a 0.5 inch stainless steel die and pressed with a laboratory press (Model C, Carver Inc., Menomonee Falls, WIS) into discs for sintering later. The applied force to the single action die was, for most powders, 5,200 lbs. (26,480 psi). For several powders with surface area above 50 m^2/g the applied force was reduced to 3,500 lbs (17,800 psi) to avoid powder sticking to the die wall and/or delamination of the disc. The pressed discs were then placed on stabilized zirconia setter plate and sintered in air at temperatures of 1200°C to 1450°C for 2 to 4 hours. For sintering temperatures of 1320°C or below, sintering was done in a batch kiln with MoSi2 heating elements (Model 305, Cladan Technology, San Marcos, CA). For sintering temperatures above 1320°C and up to 1450°C , sintering was done with a small laboratory batch furnace with MoSi2 heating elements (CM Rapid Temperature Furnace, Bloomfield, NJ). Temperature ramp up rate and cooling rate of 200°C/hr was used. These sintered smaller diameter discs were used to study the basic ceramic properties such as shrinkage, density, grain size etc. For selected compositions, large diameter discs were pressed using a 1.125 inch diameter stainless steel die. In this case, 10 to 15 grams of powder with binder solution was loaded into the die and single action pressed at 5,200 lbs. (5,230 psi) into large diameter discs. These discs were then place on stabilized zirconia setter plate and sintered at 1200°C to 1450°C for 4 hours. Same kilns as mentioned above were used. Because of much more mass of the large diameter discs, slower temperature ramp up rate and cooling rate of 100°C/hr was used. Also, soak time at the sintering temperature was increased to 4 hours. At Alfred University, sintered large diameter discs were cut into bars for thermoelectric property measurement.

In the proposal, it was proposed that the air sintered samples be annealed up to 900°C in H2/Ar gas before thermoelectric measurement. It was then decided that it would be better to sinter the samples in H2/Ar gas mixture from 1200°C to 1450°C instead.

For sintering in reduced atmosphere, 10 grams of each reacted powder composition was ground by hand in an agate mortar and pestle to break up any agglomerates. 1 ml of a 10 wt% aqueous polyvinyl alcohol (PVA) solution (Celvol 21205, Celanese Ltd, Dallas, TX) was added into the powder and mixed with the mortar and pestle until homogeneous; about 5 minutes. The powder/binder mixture was granulated by repeatedly cutting with a rubber spatula and then dried in an oven at 65°C for 15 minutes. Nominally 6 grams of powder was pressed into a 1.0 inch diameter cylindrical pellet using a tungsten carbide-faced die and laboratory press (model #3925, Carver Inc., Wabash, IN) to 5,000 psi. The pellets were vacuum sealed in lubricant-free latex condoms and isopressed to 20,000 psi (Autoclave Engineers, model #IP-6-23-30). The pellets were placed on 99.9% alumina plates inside a 3 inch diameter controlled atmosphere tube furnace (model #59256-P-COM, Lindberg, Watertown, WI) which was purged with 4%H_2/96%Ar gas. Gas flow during a sintering run was 150 ml/min. The sample temperature was monitored with a type R thermocouple placed near the pellets. The standard heating schedule was heating at 3°C/min to a peak temperature which depended upon the composition,

a 1 hour hold and then cooling to room temperature at 3°C/min. The sintered density was calculated from measured pellet mass and geometrical dimensions.

4.1.3 Testing of Discs

After sintering, the thickness, diameter, dry weight in air, and immersed weight in water of small diameter discs were measured to calculate their shrinkage, density, and porosity. Grain size was examined by SEM (Hitachi FE-SEM SU-70).

Large diameter discs were submitted to Alfred University for thermoelectric properties measurements by 4-probe technique. The measurements were performed with either a single sample or a triple sample set up.

For single sample set up, pellets were cut into rectangular shapes of 3mm×4mm×12mm (a × b × L). Two small grooves (0.01" wide) were cut into the sample surface at ¼ and ¾ of the length (L) of bars to prevent slippage of the inner electrode wires using in the four-point electrical measurements. The bar-shaped sample with gold inner electrode wires was loaded into a tube furnace (Model 2100 Tube furnace, Thermolyne, USA). The sample was mechanically compressed between two outer (current) electrodes attached to R-type thermocouples (Pt-13% Rh/Pt, 0.01" diameter). Gold foil (0.01" thick) was used for the outer electrodes. Two inner electrodes consisting of R-type thermocouples are held in contact with the sample by means of gold wire (0.01" diameter) wrapped around the sample.

A new triple sample set-up was constructed to increase the number of samples that could be tested. In the new set up, the bottom platform of a bottom-loading dome furnace (Whip Mix dental furnace) was designed to accommodate three sets of four spring-loaded thermocouples placed at 120 degree intervals surrounding a center SiC heater, as illustrated in Fig. 1

Bar shaped samples 2mmx4mmx16mm (axbXL) were placed on top of a set of four spring-loaded thermocouples and held in place with additional spring-loaded compression applied from the top. The center SiC heater was used to provide a thermal gradient across the sample.

Simultaneous DC conductivity and thermopower measurements were conducted at 200 ~ 900°C. In these experiments, measurements were conducted in the air using a Labview-controlled system consisting of a programmable current source (Model 2400 Sourcemeter, Keithley Instruments, USA), and a voltage/current meter (Model 2700 Multimeter/DATA ACQUISTION, Keithley Instruments, USA).

Electrical measurements were recorded at each temperature after equilibrium was achieved as judged by observing conductivity as function of time. To correct for the thermopower contributions, an average conductivity was calculated from measurements collected in forward and reverse directions. Thermopower measurements were conducted using the 'steady state straddle' method. In the single sample set up, the sample was placed in the natural temperature gradient of the furnace to provide 10-20°K gradient along the length of the sample. For the triple sample set up, the center heater provided a 50-100°K gradient along the length of the sample. Temperatures were measured at each thermocouple contact(T_1, T_2, T_3, T_4), and voltage was measured across the platinum legs of the six thermocouple combinations(V_1-V_2, V_1-V_3, V_1-V_4, V_2-V_3, V_2-V_4, and V_3-V_4). Thermoelectric coefficients were obtained by measuring the voltage drop for the temperature gradient along the sample length. The thermoelectric coefficient, or Seebeck coefficient, Q is defined as Eq. (1)

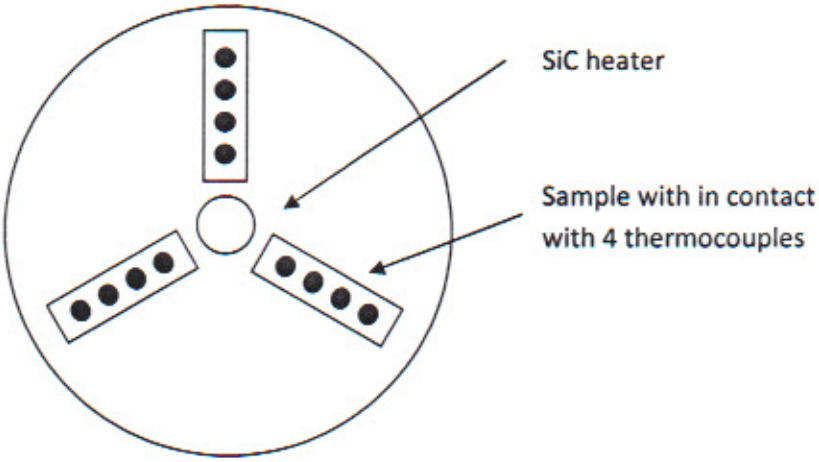

Fig. 1 Schematic of a Triple Sample Holder for 4-probe Measurement

$$Q = \lim_{\Delta T \to 0} \frac{\Delta V}{\Delta T} \tag{1}$$

Measured values were corrected to account for contributions from the platinum electrodes, the measured coefficient was corrected using Eq. (2)

$$Q_S = Q_M + Q_{Pt} \tag{2}$$

where, Q_s is the corrected coefficient, Q_m is the measured coefficient, Q_{pt} is thermoelectric coefficient of platinum.

4.1.4 Results and Discussion

Table 5 lists basic physical properties of small diameter discs sintered in air. In most cases, disc samples were sintered at multiple temperatures. The physical data for discs sintered at the lowest temperature gave representative shrinkage, density and grain size values are shown in Table 5. Table 6 lists the grain size analysis for discs sintered in air. Table 7 lists the thermoelectric data at near 700°C (973°K) of discs sintered in air, or in H2/Ar, or both. Note that samples 002, 003, 010, and 011 were not tested for their thermoelectric properties because of their poor sintering. Samples 019, 020, and 021 were also not tested for their thermoelectric properties because of their too large grain sizes.

Sample No.	Group	Composition	Sintering	Shrinkage (%)	Density (g/cc)	Porosity (%)
001	1	0.8 TiO2 - 0.2 TaO2.5	1450C/2H, Air	17.80	5.41	5.58
002	1	0.6 TiO2 - 0.4 TaO2.5	1450C/2H, Air	14.50	5.67	8.13
003	1	0.4 TiO2 - 0.6 TaO2.5	1450C/2H, Air	8.40	6.37	25.81
004	1	0.8 TiO2 - 0.2 NbO2.5	1450C/2H, Air	16.40	4.37	9.13
			1360C/2H, Air	16.60	4.30	4.66
005	1	0.6 TiO2 - 0.4 NbO2.5	1450C/2H, Air	15.20	4.33	7.69
			1360C/2H, Air	15.60	4.26	4.53
006	1	0.4 TiO2 - 0.6 NbO2.5	1450C/2H, Air	15.20	4.38	8.28
			1360C/2H, Air	15.20	4.32	5.09
039	1	0.97 TiO2 - 0.03 Nb2O2.5	1320C/2H, Air	15.80	4.31	5.04
			1450C/4H, Air	17.40	4.37	7.19
015	1	0.98 TiO2 - 0.02 CuO	1300C/2H, Air	12.60	3.91	4.57
016	1	0.96 TiO2 - 0.04 CuO	1300C/2H, Air	14.40	3.99	4.79
017	1	0.94 TiO2 - 0.06 CuO	1300C/2H, Air	14.80	3.98	6.23
019	1	0.98 TiO2 - 0.02 LiO0.5	1200C/2H, Air	18.60	3.92	4.61
020	1	0.95 TiO2 - 0.05 LiO0.5	1200C/2H, Air	18.40	3.84	6.40
021	1	0.92 TiO2 - 0.08 LiO0.5	1200C/2H, Air	17.60	3.73	5.60
007	2	0.98 CeO2 - 0.02 NbO2.5	1450C/2H, Air	16.60	7.14	4.58
008	2	0.96 CeO2 - 0.04 NbO2.5	1450C/2H, Air	16.60	7.14	5.22
009	2	0.94 CeO2 - 0.06 NbO2.5	1450C/2H, Air	16.80	7.23	7.98
044	2	0.874 CeO2 - 0.126 NbO2.5	1320C/2H, Air	16.00	6.79	4.90
012	2	0.98 CeO2 - 0.02 CuO	1450C/2H, Air	12.80	6.83	12.82
013	2	0.96 CeO2 - 0.04 CuO	1450C/2H, Air	12.40	6.87	14.89
014	2	0.94 CeO2 - 0.06 CuO	1450C/2H, Air	12.00	7.03	18.52
010	3	3 SrO - TiO2 - NbO2.5	1450C/2H, Air	7.20	5.13	36.09
011	3	3 SrO - TiO2 - TaO2.5	1450C/2H, Air	0.00	5.38	57.52
040	3	1.0 SrO - 0.8 TiO2 - 0.2 NbO2.5	1450C/4H, Air	14.40	4.81	28.46

Table 5 (Part I) Shrinkage, Density, and Porosity of Discs Sintered in Air

Sample No.	Group	Composition	Sintering	Shrinkage (%)	Density (g/cc)	Porosity (%)
018	4	0.5 BaO - 0.5 SrO - 0.6 CoO - 0.4 FeO1.5	1200C/2H, Air	25.20	5.30	7.15
			1240C/2H, Air	25.20	5.33	7.13
			1280C/2H, Air	28.40	4.57	17.17
022	4	CaMnO3	1320C/2H, Air	19.60	4.71	4.95
023	4	CaMnO3 - BaTiO3 - Nb2O5 - CoO	1320C/2H, Air	15.20	4.81	6.22
024	4	CaMnO3 - CeO2 - NbO2.5	1320C/2H, Air	16.20	5.00	13.14
025	4	CaMnO3 - TiO2 - Nb2O5	1320C/2H, Air	18.20	4.34	5.57
026	4	CaMnO3 - BaTiO3	1320C/4H, Air	15.80	6.08	8.63
028	4	CaCo(3)Ti(4)O12	1320C/4H, Air	13.80	4.16	10.09
041	5	SrO - 0.6 CoO - 0.4 FeO1.5	1320C/2H, Air	Lost	Lost	Lost
042	5	0.2 SrO - 0.4 NiO - 0.4 FeO1.5 - TiO2	1360C/2H, Air	16.00	4.64	5.04
043	5	0.2 CaO - 0.4 NiO - 0.4 FeO1.5 - TiO2	1360C/2H, Air	15.00	4.45	8.65
029	6	X7R302H	1320C/4H, Air	15.40	6.13	6.90
030	6	NPO610H	1280C/2H, Air	18.40	5.86	11.55
031	6	COG600H	1280C/2H, Air	17.60	5.64	2.25
032	6	COG350H	1280C/2H, Air	17.80	5.96	5.06
033	6	BaTiO3	1450C/2H, Air	16.20	5.87	9.63
034	6	COG630L	1140C/2H, Air	17.60	5.69	2.76
035	6	Y5V163L	1140C/2H, Air	17.00	6.34	5.91
036	6	Z5U113H	1320C/4H, Air	15.20	5.51	4.52
037	6	X7R302H - Ba(0.5)Sr(0.5)Co(0.6)Fe(0.4)O3	1360C/2H, Air	12.20	5.04	6.25

Table 5 (Continued, Part II) Shrinkage, Density, and Porosity of Discs Sintered in Air

Sample	Group	Composition	Sintering	Microstructure Description
001	1	0.8 TiO2 - 0.2 TaO2.5	1450C/2H, Air	Brick like grains with sharp edges and corners, 6 - 10 microns
002	1	0.6 TiO2 - 0.4 TaO2.5	1450C/2H, Air	Did not sinter well
003	1	0.4 TiO2 - 0.6 TaO2.5	1450C/2H, Air	Did not sinter
004	1	0.8 TiO2 - 0.2 NbO2.5	1450C/2H, Air	Plate like grains, up to 30 microns + Long needle like grains, up to 40 microns
			1360C/2H, Air	Plate like grains, up to 10 microns + Long needle like grains, up to 20 microns
005	1	0.6 TiO2 - 0.4 NbO2.5	1450C/2H, Air	Plate like grains, up to 30 microns + Long needle like grains, up to 40 microns
			1360C/2H, Air	Plate like grains, up to 2 - 4 microns + Long needle like grains, 6 - 8 microns
006	1	0.4 TiO2 - 0.6 NbO2.5	1450C/2H, Air	Large grains, > 30 microns coated with liquid phase
			1360C/2H, Air	Plate like grains, up to 4 microns + Long needle like grains, up to 8 microns
039	1	0.97 TiO2 - 0.03 Nb2O2.5	1320C/2H, Air	Brick like grains with sharp edges and corners, 6 - 8 microns
039			1320C/2H, Air	Brick like grains with sharp edges and corners, 6 - 8 microns
039			1450C/4H, Air	Brick like grains with sharp edges and corners, 6 - 8 microns
015	1	0.98 TiO2 - 0.02 CuO	1300C/2H, Air	Large elongated grains, > 50 microns + liquid phase in grain boundaries
016	1	0.96 TiO2 - 0.04 CuO	1300C/2H, Air	Large elongated grains, > 50 microns + liquid phase in grain boundaries
017	1	0.94 TiO2 - 0.06 CuO	1300C/2H, Air	Large elongated grains, > 50 microns + liquid phase in grain boundaries
019	1	0.98 TiO2 - 0.02 LiO0.5	1200C/2H, Air	Very Large Grains, > 50 microns
020	1	0.95 TiO2 - 0.05 LiO0.5	1200C/2H, Air	Very Large Grains, > 50 microns
021	1	0.92 TiO2 - 0.08 LiO0.5	1200C/2H, Air	Very Large Grains, > 50 microns
007	2	0.98 CeO2 - 0.02 NbO2.5	1450C/2H, Air	Large grains, 10 - 20 microns, + small 5 micron grains embedded at triple points
008	2	0.96 CeO2 - 0.04 NbO2.5	1450C/2H, Air	Large grains, 10 - 30 microns + small grains, 5-10 microns embedded at triple points
009	2	0.94 CeO2 - 0.06 NbO2.5	1450C/2H, Air	Grains of 4 - 8 microns
044		0.874 CeO2 - 0.126 Nb2O5	1320C/2H, Air	Grains of 1 - 4 microns
012	2	0.98 CeO2 - 0.02 CuO	1450C/2H, Air	Very large grains, 20 - 30- microns
013	2	0.96 CeO2 - 0.04 CuO	1450C/2H, Air	Very large grains, 10 - 30 microns
014	2	0.94 CeO2 - 0.06 CuO	1450C/2H, Air	Very large grains, 10 - 20 microns
010	3	3 SrO - TiO2 - NbO2.5	1450C/2H, Air	Did not sinter
011	3	3 SrO - TiO2 - TaO2.5	1450C/2H, Air	Did not sinter
040	3	1.0 SrO - 0.8 TiO2 - 0.2 NbO2.5	1450C/4H, Air	Round grains, 6-10 microns
018	4	0.5 BaO - 0.5 SrO - 0.6 CoO - 0.4 FeO1.5	1280C/2H, Air	Very large grains, > 50 microns, coated with liquid phase.
			1200C/2H, Air	Sharp edged gains, 6 - 8 microns, + small smooth grains, 2 microns
			1240C/2H, Air	Very large grains, 30 - 50 microns
022	4	CaMnO3	1320C/2H, Air	Grains, 4 - 10 microns + grains, 2 microns
023	4	CaMnO3 - BaTiO3 - Nb2O5 – CoO	1320C/2H, Air	Gains, 2 - 3 microns + small second phase grains, 1 micron.
024	4	CaMnO3 - CeO2 - Nb2O5	1320C/2H, Air	Grains, 2 - 3 microns, partially fused together
025	4	CaMnO3 - TiO2 - Nb2O5	1320C/2H, Air	Grains, 2 - 3 microns, partially fused together
026	4	CaMnO3 - BaTiO3	1320C/4H, Air	Very large grains, 30 - 40 microns
028	4	CaCo(3)Ti(4)O12	1320C/4H, Air	Square grains, 6 - 10 microns
041	5	SrO - 0.6 CoO - 0.4 FeO1.5	1320C/2H, Air	Very large and non uniform grains, 20 - 50 microns
042	5	0.2 SrO - 0.4 NiO - 0.4 FeO1.5 - TiO2	1360C/2H, Air	Large and non uniform grains coated with liquid phase
043	5	0.2 CaO - 0.4 NiO - 0.4 FeO1.5 - TiO2	1360C/2H, Air	Large 10 - 20 microns cubic grains + small < 5 micron grains + Needles, 10 - 30 microns
029	6	X7R302H	1320C/4H, Air	Small round grins, < 1 micron
030	6	NPO610H	1280C/2H, Air	Square gains, 1 - 2 microns + needle grains 2 - 3 microns
031	6	COG600H	1280C/2H, Air	Square grains, 1 - 2 microns + needle grains, 1 - 3 microns
032	6	COG350H	1280C/2H, Air	Grains, 2 - 5 microns + hexagonal grains, 8 - 10 microns
033	6	BaTiO3	1450C/2H, Air	Very large grains, 40 - 100 microns
034	6	COG630L	1140C/2H, Air	Square grains, 1 - 2 microns + Long needle grains, 2 - 3 microns
035	6	Y5V163L	1140C/2H, Air	Grains, 3 - 4 microns
036	6	Z5U113H	1320C/4H, Air	Smooth grains, 4 - 6 microns
037	6	X7R302H - Ba(0.5)Sr(0.5)Co(0.6)Fe(0.4)O3	1360C/2H, Air	Large grains, 4 - 15 microns

Table 6 Grain Size Analysis of Discs Sintered in Air

Sample No.	Group	Composition	Sintering	Temperature (K)	Seebeck Coefficient (μV/K) Near 700C	Electrical Conductivity (S/cm) Near 700C	Power Factor (Watt/mK^2) Near 700C
001	1	0.8 TiO2 - 0.2 TaO2.5	1450C/4H, Air	990	-419	1.33E-01	2.33E-06
			1350C/1H, H2/Ar	974	-202	5.63E+01	2.30E-04
004	1	0.8 TiO2 - 0.2 NbO2.5	1250C/4H, Air	990	-886	7.02E-04	5.51E-08
			1232C/1H, H2/Ar	958	-309	2.70E-01	2.58E-06
005	1	0.6 TiO2 - 0.4 NbO2.5	1250C/4H, Air	985	-845	2.03E-03	1.42E-07
			1232C/1H, H2/Ar	958	-188	1.31E+01	4.62E-05
006	1	0.4 TiO2 - 0.6 NbO2.5	1250C/4H, Air	988	-725	5.06E-03	2.63E-04
			1232C/1H, H2/Ar	973	-313	8.85E-01	8.67E-06
039	1	0.97 TiO2 - 0.03 NbO2.5	1450C/4H, Air	944	-331	5.36E-01	5.87E-06
			1320V/4H, Air	961	-421	5.10E-01	9.04E-06
			1320C/1H, H2/Ar	967	-239	1.13E+01	6.45E-05
015	1	0.98 TiO2 - 0.02 CuO	1150C/4H, Air	996	NA	8.77E-05	NA
			1350C/1H, H2/Ar	758	-299	6.54E+00	5.85E-05
016	1	0.96 TiO2 - 0.04 CuO	1150C/2H, Air	994	-133	1.90E-04	3.36E-10
			1350C/1H, H2/Ar	941	-679	3.42E-02	1.58E-06
017	1	0.94 TiO2 - 0.06 CuO	1150C/2H, Air	1079	-65	4.96E-04	2.06E-10
			1350C/1H, H2/Ar	861	-446	3.72E-01	7.40E-06
019	1	0.98 TiO2 - 0.02 LiO0.5	1200C/2H, Air	NA	NA	NA	NA
020	1	0.95 TiO2 - 0.05 LiO0.5	1200C/2H, Air	NA	NA	NA	NA
021	1	0.92 TiO2 - 0.08 LiO0.5	1200C/2H, Air	NA	NA	NA	NA
007	2	0.98 CeO2 - 0.02 NbO2.5	1450C/4H, Air	988	-577	2.74E-01	9.14E-06
			1400C/1H, H2/Ar	969	-566	1.05E-01	3.35E-06
008	2	0.96 CeO2 - 0.04 NbO2.5	1450C/2H, Air	NA	NA	NA	NA
			1400C/1H, H2/Ar	938	-595	5.25E-02	1.86E-06
009	2	0.94 CeO2 - 0.06 NbO2.5	1450C/2H, Air	NA	NA	NA	NA
			1400C/1H, H2/Ar	945	-591	6.16E-02	2.15E-06
044	2	0.874 CeO2 - 0.126 NbO2.5	1320C/2H, Air	NA	NA	NA	NA
			1320C/4H, Air	953	-350	9.41E-02	1.15E-06
012	2	0.98 CeO2 - 0.02 CuO	1450C/2H, Air	NA	NA	NA	NA
013	2	0.96 CeO2 - 0.04 CuO	1450C/2H, Air	NA	NA	NA	NA
014	2	0.94 CeO2 - 0.06 CuO	1450C/2H, Air	NA	NA	NA	NA
010	3	3 SrO - TiO2 - NbO2.5	1450C/2H, Air	NA	NA	NA	NA
011	3	3 SrO - TiO2 -TaO2.5	1450C/2H, Air	NA	NA	NA	NA
040	3	1.0 SrO - 0.8 TiO2 - 0.2 NbO2.5	1450C/4H, Air	985	-409	9.70E-03	1.62E-07
			1450C/1H, H2/Ar	973	-305	2.75E-06	2.56E-11
018	4	0.5 BaO - 0.5 SrO - 0.6 CoO - 0.4 FeO1.5	1280C/2H, Air	959	82	1.61E-01	1.09E-05
			1220C/2H, Air	965	121	8.63E+00	1.26E-05
022	4	CaMnO3	1320C/4H, Air	NA	NA	NA	NA
			1320C/4H, Air	968	-279	8.48E+00	6.60E-05
023	4	CaMnO3 - BaTiO3 - Nb2O5 – CoO	1320C/4H, Air	NA	NA	NA	NA
			1300C/1H, H2/Ar	952	-209	1.30E+00	5.68E-06
024	4	CaMnO3 - CeO2 - Nb2O5	1320C/4H, Air	963	-38	5.86E+01	8.33E-06
025	4	CaMnO3 - TiO2 - Nb2O5	1320C/4H, Air	978	-72	6.91E-02	3.53E-08
026	4	CaMnO3 - BaTiO3	1320C/4H, Air	956	-851	9.74E-04	7.05E-08
027	4	Ca3Co4O9	1320C/2H, Air	911	334	1.82E-02	2.03E-06
028	4	CaCo(3)Ti(4)O12	1320C/4H, Air	941	847	1.49E-03	1.07E-07

Table 7 (Part I) Thermoelectric Properties of Samples

Sample No.	Group	Composition	Sintering	Temperature (K)	Seebeck Coefficient (μV/K) Near 700C	Conductivity (S/cm) Near 700C	Power Factor (Watt/mK^2) Near 700C
041	5	SrO - 0.6 CoO - 0.4 FeO1.5	1320C/2H, Air	933	26	3.36E+01	2.19E-06
042	5	0.2 SrO - 0.4 NiO - 0.4 FeO1.5 - TiO2	1360C/2H, Air	978	-340	1.03E-01	1.26E-06
043	5	0.2 CaO - 0.4 NiO - 0.4 FeO1.5 - TiO2	1360C/2H, Air	753	-470	2.87E-03	6.63E-08
029	6	X7R302H	1320C/4H, Air	928	-1050	1.51E-05	1.66E-09
			1320C/1H, H2/Ar	972	-280	6.44E+00	5.05E-05
030	6	NPO610H	1280C/4H, Air	990	-1390	7.70E-06	1.49E-09
031	6	COG600H	1280C/4H, Air	947	NA	1.18E-05	NA
032	6	COG350H	1280C/4H, Air	NA	NA	NA	NA
033	6	BaTiO3	1450C/2H, Air	968	963	5.97E-04	5.54E-08
034	6	COG630L	1140C/4H, Air	NA	NA	NA	NA
035	6	Y5V163L	1140C/4H, Air	1041	961	1.09E-03	1.01E-07
036	6	Z5U113H	1320C/4H, Air	991	941	5.64E-04	4.99E-08
			1320C/4H, H2/Ar	993	129	7.68E-03	3.50E-07
037	6	X7R302H - Ba(0.5)Sr(0.5)Co(0.6)Fe(0.4)O3	1360C/4H, Air	948	220	8.17E-02	3.95E-07

Table 7 (Continued, Part II) Thermoelectric Properties of Samples

Seebeck coefficients and electrical conductivities of samples as a function of temperature were also measured. It was observed, for most of the samples, that electrical conductivity is the most temperature dependent parameter. It increases with temperature exponentially indicating a thermally activated process in these materials. Seebeck coefficient is also dependent on temperature but not in an exponential manner. As an example, Fig. 2 and Fig 3 show Seebeck coefficient and electrical conductivity vs. temperature of Sample 039.

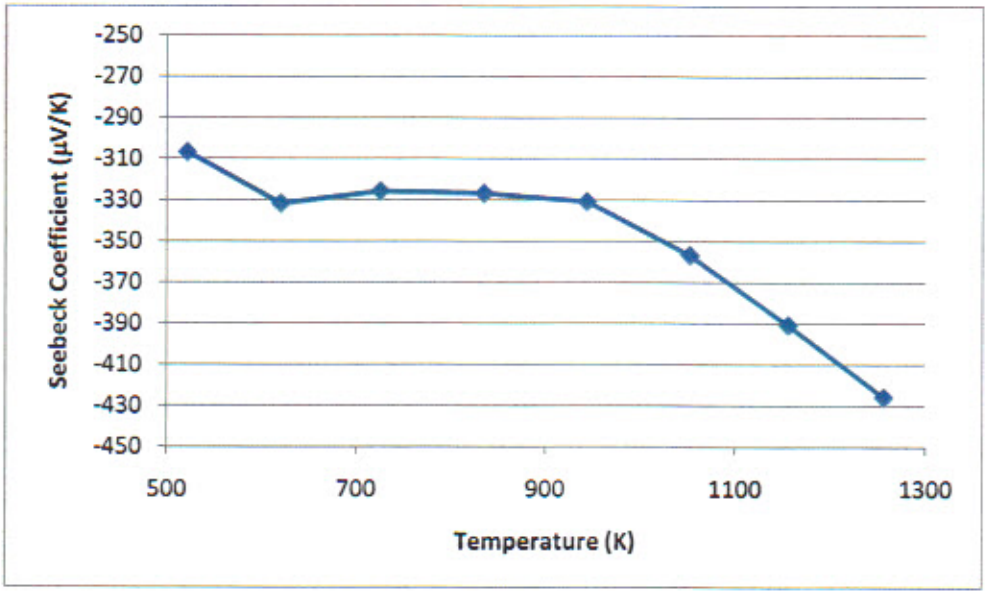

Fig. 2 Seebeck Coefficient as a Function of Temperature for Sample 039

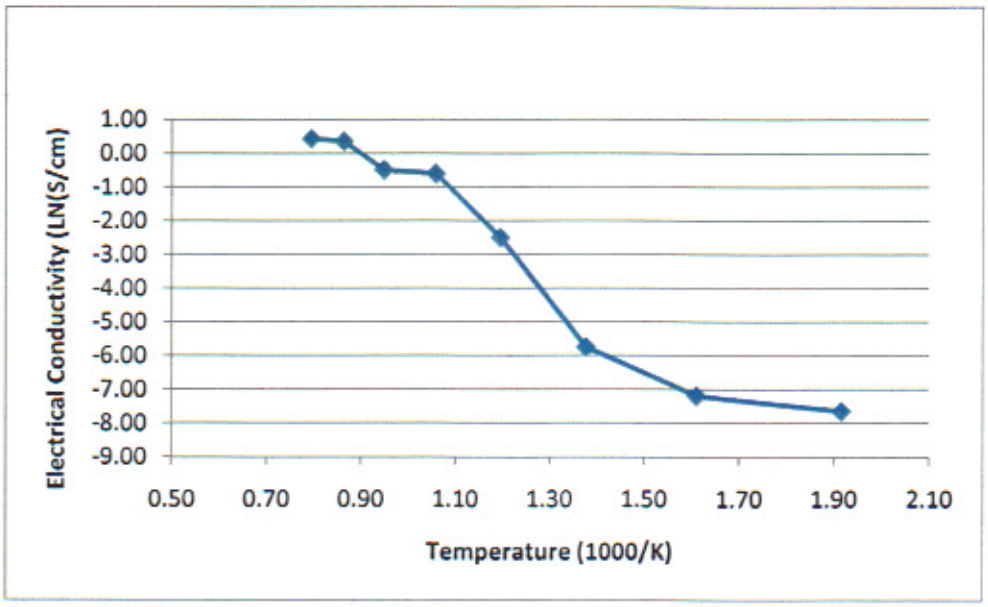

Fig. 3 Natural Logarithm of Electrical Conductivity as a Function of Temperature for Sample 039

The performance of a thermoelectric material is normally evaluated by its power factor, PF, and its figure of merit, ZT.

Power factor, PF, is defined as,

$$PF = Q^2 \times \sigma \quad (3)$$

Figure of merit, ZT, is defined as,

$$ZT = (Q^2 \times \sigma \times T)/k \quad (4)$$

Where in equations (3) and (4), Q is the Seebeck coefficient (μV/K), σ is the electrical conductivity (S/cm), T is the absolute temperature (°K), and k is the thermal conductivity (Watt/mK). PF has a unit of (Watt/mK^2) and ZT is dimensionless.

In cases where the thermal conductivity data is not available, one can use ZT x k as an alternative parameter to evaluate the material since k usually is not too much temperature dependent. Fig. 4 shows ZTxThermal Conductivity of Sample 039 which should have a similar appearance as if one would plot ZT vs. temperature.

Overall observation of thermoelectric data shown in Table 7 indicates that Seebeck coefficients (Q, μV/K) of all samples are from -100 μV/K to -1000 μV/K for both n-type and p type materials. These Seebeck coefficient values are in the same order of magnitude as most of the reported oxide thermoelectric materials of various kinds. However, their electrical conductivities (σ, S/cm) are very low. Therefore, their power factors (PF, Watt/mK^2) and figure of merits (ZT) are also very low. It is estimated that for materials with Seebeck coefficients around +/- 100 to +/- 1000 μ/K, their electrical conductivity values should be at least higher than 100 S/cm in order to achieve ZTs > 0.1. Conductivities of samples listed in Table 7, except for several samples (Sample 001, 005, 039, 018, 022 and 024) are at least two orders of magnitude below 100 S/cm.

It is felt that conductivities of these samples have to be increased to much higher values first before selection of materials can be made for future material development and module design.

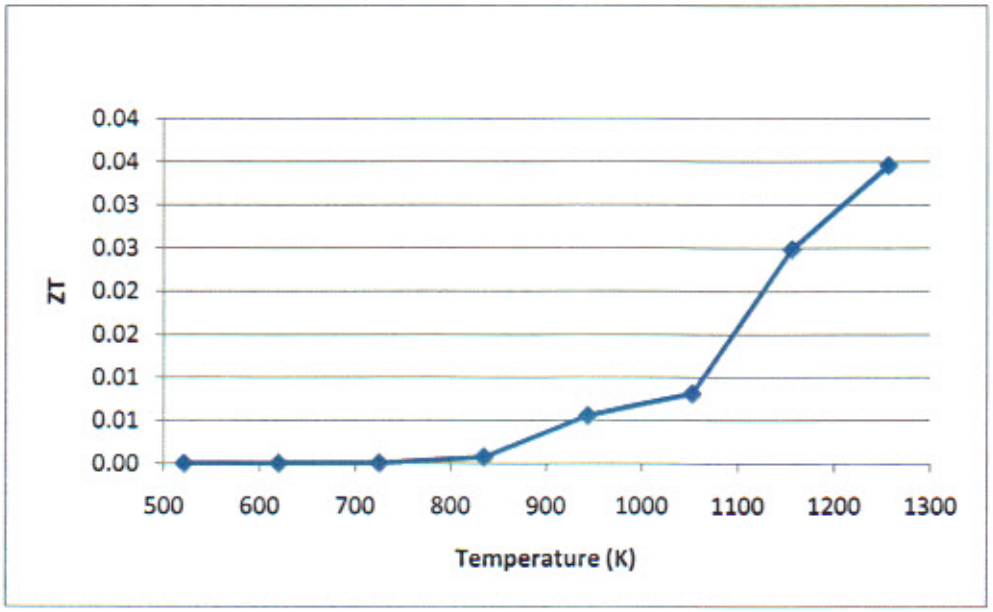

Fig. 4 ZT x Thermal Conductivity as a Function of Temperature for Sample 039

One of the reasons why the electrical conductivities and power factors of these samples are so low might be that these samples were only sintered by conventional technique either in air or in reducing atmosphere in H2/Ar gas mixture. This sintering process apparently could not yield sufficient electrical conductivities even though samples sintered in H2/Ar had higher (but not high enough) conductivities. A different type of sintering technique may have to be employed to process these materials. Through literature search and discussion with experts in the field a recently developed Spark Plasma Sintering (SPS) technique came into mind. Although a theoretical modeling explaining how and why it worked has not been offered anywhere, SPS technique has been reported in literature to have successfully sintered the thermoelectric materials and yield much higher electrical conductivities [23-26].

Discussions of results and decisions specific to individual group of materials are presented in the following.

Group 1 (Doped TiO2): The one sample (001), which is 0.8 TiO2 – 0.2 TaO2.5 gave the best electrical conductivity and power factor among all samples studied. It is estimated that above 600°K, ZT of > 0.1 can be achieved with this material. However higher TaO2.5 doped samples (002, 003) had difficulty to sinter even at 1450°C. The TaO2.5 doping concentration will be explored later to find if an optimum level exists. The NbO2.5 doped samples also show conductivities comparable with TaO2.5 doped samples. Except for Li2O3 doped TiO2 samples, firing temperatures of Group 1 materials are from 1300°C to 1450°C. The grain structure of NbO2.5 doped samples had mixed shape of plate like grains and long needle like grains indicating likely mixed phases or crystal structures. As expected, TaO2.5 and NbO2.5 doped materials exhibits n-type behavior with Seebeck coefficients of -200 to -400 μV/K. The CuO doped samples did not result p-type behavior. They exhibit actually n-type behavior. Their

microstructure is poor. It showed large elongated grains with lots of liquid phase materials. Electrical conductivities of these samples are all very low. The Li2O3 doped samples had very low sintering temperatures (< 1200°C) and had very large grain sizes (> 50 μm), therefore these were not tested for thermoelectric properties. Electrical conductivities of CuO doped samples are all very low. Decision on Group 1 material study is to follow up further with TaO2.5 and NbO2.5 doped compositions with more details later. A material with a composition of 0.97 TiO2 – 0.03 NbO2.5 was made and evaluated by a third party company. It showed encouraging results. More details are reported later. The Li2O3 and CuO doped compositions will not be followed further. To convert TiO2 into p-type behavior, some other dopants with valence less than +4 such as Y2O3, La2O3, Na2O, or K2O will be investigated in the future.

Group 2 (Doped CeO2): Firing temperatures for Group 2 materials are near 1400°C. Seebeck coefficients are around -500 to -600 μV/K. But again, electrical conductivities are very low. Grain sizes of all samples were very large and not uniform. CuO doped samples were not tested for their thermoelectric properties. It was also observed that samples sintered at reduced atmosphere will reoxidize during thermoelectric property measurements in air. This implies that doped CeO2 compositions should be used in inert or sealed environment and likely not cost effective. Decision on Group 2 material study is not to follow further.

Group 3 (SrTiO3 and Doped SrTiO3): The two compositions selected, Sample 010 and Sample 011, would not sinter even at 1450°C. The reason could be that the compositions were too much Sr excess. Sample 040 composition (1.0 SrO – 0.8 TiO2 – 0.2 NbO2.5) does not show high enough electrical conductivity when sintered in air. However, this composition system was recommended by experts in the field. Decision on Group 3 material study is therefore to follow up the 1.0 SrO – 0.8 TiO2 – 0.2 NbO2.5 system in more details in Task 3 and Task 4. Also, it is planned to investigate the feasibility of converting this composition system into p-type behavior by replacing NbO2.5 with p-type dopants such as Y2O3, La2O3, Li2O3, K2O, and CuO etc. If successful, n-type and p-type materials with more thermal matching and more processing compatibility may be achievable.

Group 4 (CoO and MnO2 Based Formulations): Sample 018 (0.5 BaO – 0.5 CaO – 0.6 CoO – 0.4 FeO1.5), Sample 027 (Ca3Co4O9), and Sample 028 (CaCo(3)Ti(4)O12) all show p-type behavior with Seebeck coefficients of about +80 μV/K +330 μV/K and +850 μV/K. Sample 027 (Ca3Co4O9) appears to have the best combination of Seebeck coefficient and electrical conductivity although the actual value of electrical conductivity is, like others, still low. The MnO2 based samples, Samples 022, 024, 025, and 026 showed n-type behavior with Seebeck coefficients around -50 to -800 μV/K. The electrical conductivities of these samples appear to be a bit higher than the other groups of samples but the actual values are still very low. The issue here, again, might be the sintering technique. Grain sizes of these samples are difficult to determine since there were lots of second and liquid phases present. Sintering temperatures of this Group 4 materials appear to be lower and yet shrinkages appear to be higher than Group 1 and Group 2 materials. This might present compatibility and matching issues later when n-type and p-type materials are cosintered in a module design. Decision on Group 4 material study is to follow up this material system only if development of p-type materials from other composition systems proves difficult.

Group 5 (CoO, Fe2O3, SrO, NiO Based Formulations): The SrO - 0.6 CoO – 0.4 FeO1.5 (Sample 041) exhibited a small p-type but very low Seebeck coefficient (25 μV/K). It seems like most of the cobaltite compounds are p-type. The electrical conductivity of Sample 041 was higher,

above 30 S/cm. But, because of the low Seebeck coefficient, the overall power factor is still low. The 0.2 SrO - 0.4 NiO – 0.4 FeO1.5 – TiO2 (Sample 042) and 0.2 CaO - 0.4 NiO – 0.4 FeO1.5 – TiO2 (Sample 043) compositions are both n-type. Seebeck coefficients are about -350 μV/K to -470 μV/K. The SrO containing sample (Sample 042) had higher electrical conductivity than the CaO containing sample (Sample 043). However, actual conductivity value of Sample 043 was still low and its power factor is also low. All three samples had very large grain sizes and non-uniform grain size distributions. Decision on Group 5 material study is not to follow these materials further.

Group 6 (Dielectric Formulations): Results of this group are interesting. When sintered in air, Sample 029 (X7R302H) and Sample 030 (NPO610H) showed n-type behavior with high Seebeck coefficients of more than -1000 μV/K. Sample 033 (BaTiO3), Sample 035 (Y5V153L), and Sample 036 (Z5U113H) showed p-type behavior with high Seebeck coefficients around + 950 μV/K. X7R302H is a temperature stable dielectric formulation (Meets EIA X7R specifications) with a dielectric constant of around 3000. The composition is mainly BaTiO3 with a small amount of additives. NPO610H is an ultra temperature stable dielectric formulation (Meets EIA NPO specifications) with a dielectric constant of about 60. The composition is based on rare earth titanate. Y5V153L and Z5U113H are all high dielectric constant compositions (Meets EIA Y5V and Z5U specifications) with dielectric constant of about 16,000 and 12,000. The compositions are BaTiO3 + BaZrO3 + additives. However, their electrical conductivities were very low. The low electrical conductivities were expected since they were formulated for dielectric and capacitor application. It is felt that, because of their high Seebeck coefficients, it may still be worthwhile to investigate if with some composition modification and/or processing modification they could possibly be developed as high temperature oxide thermoelectric materials. As shown in the case of Samples 029 and 036, sintering in reducing atmosphere appears to improve electrical conductivity significantly. Development of p-type thermoelectric compositions from these Group 6 materials is of particular interest because, if workable, it presents materials alternative to the current Cobaltite based p-type materials that will be more process compatible with n-type components.

During study and analysis of thermoelectric data above, it was noticed that the absolute value of Seebeck coefficient and electrical conductivity always vary in a different direction. In other words, each time electrical conductivity increases, the absolute value of Seebeck coefficient decreases. A further analysis was then conducted. In Fig. 5, The nature logarithm of the electrical conductivity, LN (σ) is plotted as a function of absolute value of the Seebeck coefficient for all the n-type samples tested. The data is a collection of Seebeck coefficients and nature logarithm of electrical conductivities of all different compositions and under all different processing conditions. It is interesting to notice that there seems to be a universal correlation between LN(σ) and Seebeck coefficient regardless of composition systems and processing conditions. It is not sure if a theoretical model can be established to explain this possible correlation. However, this data analysis suggests that it might be possible to predict Seebeck coefficient from conductivity data or vice versa.

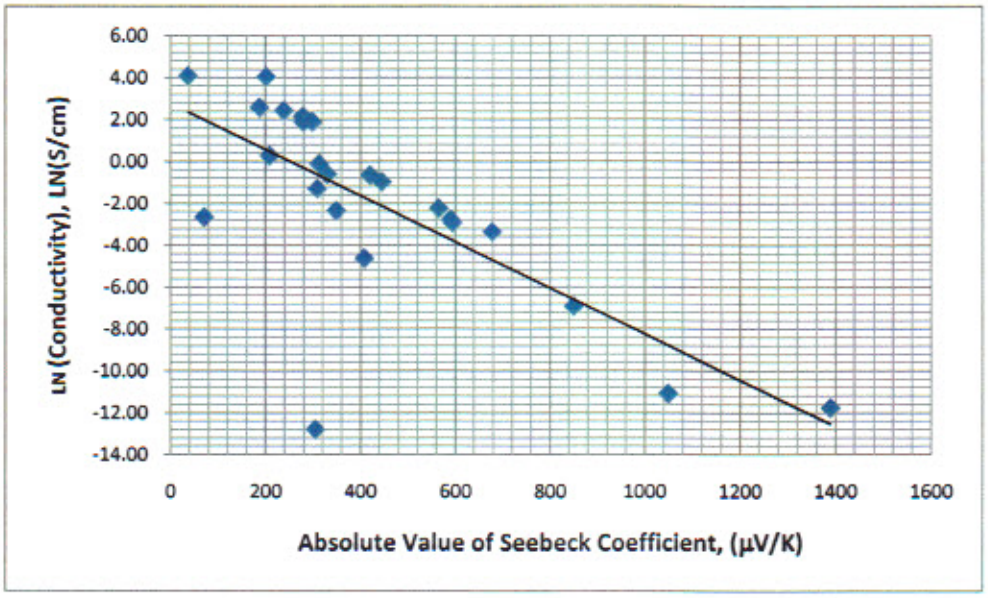

Fig. 5 Natural Logarithm of Electrical conductivity vs. Absolute Value of Seebeck Coefficient

4.2 Task 3, Characterization of Powders and Ceramics

Discussing with industry experts and university researchers pointed out that the TiO2-NbO2.5 and SrO-TiO2-NbO2.5 based compositions are two of the most technically and economically feasible oxide n-type materials for practical high temperature applications. Also, no p-type oxide materials other than Ca3Co4O9 materials are available.

During the course of Task 1 and Task 2 works, dialogs and communications were established with a leading commercial company of thermoelectric device, materials, and technology. This company who will be referred to as "Company X" for the remainder of this report is very interested in our thermoelectric material development program and view us as a potential cost effective thermoelectric powder producer. They have full lines of material processing (especially, the Spark Plasma Sintering furnace) and characterization (XRD, SEM and ICP) facilities to process, test, and analyze all fundamental properties of ceramic powders and components. More important to Phase I work is that they have full lines of equipment to measure thermoelectric properties such as Seebeck coefficient, electrical conductivity, thermal conductivity etc. They showed keen interests in the TiO2-NbO2.5 and SrO – TiO2 – NbO2.5 based formulations that we were working on under this DOE proposal. They agreed under NDA agreement to test, evaluate, and advise on powders submitted by us. We took the opportunity and submitted the 0.97 TiO2 – 0.03 NbO2.5 and 1.0 SrO – 0.8 TiO2 – 0.2 NbO2.5 powders for their initial evaluation. At Company X's request, these powders were ball milled to two different sizes around 1.0 micron. Table 8 shows a summary of their evaluation of physical properties of the two powders. Table 9 shows a summary of thermoelectric properties. Fig. 6, Fig. 7, Fig. 8, Fig. 9, Fig. 10, Fig. 11, Fig. 12, and Fig. 13 show thermoelectric properties vs. temperature. The powders were sintered by Company X by Spark Plasma Sintering.

Powder Sample ID	00187K	00187L	00183K	00183L
Composition	0.97 TiO2 - 0.03 NbO2.5	0.97 TiO2 - 0.03 NbO2.5	1.0 SrO - 0.8 TiO2 - 0.2 NbO2.5	1.0 SrO - 0.8 TiO2 - 0.2 NbO2.5
Powder Particle Size (Measured by TAM by Microtrac)				
D90 (μm)	1.62	1.20	2.30	0.91
D50 (μm)	1.02	0.83	0.87	0.65
D10 (μm)	0.65	0.57	0.55	0.51
Powder Particle Size (Measured by Company X by SEM)				
(μm)	1.2 - 1.5	0.5 - 0.8	< 5 μm agglomerates of	< 3 μm agglomerates of
			< 1 μm particles	< 1 μm particles
Major Phase (Powder)	Rutile	Rutile	SrTiO3	SrTiO3
			Sr5Nb4O15, SrNb4O6, TiO2	Sr5Nb4O15, SrNb4O6, TiO2
Impurity				
0.3 -1.0 %		Zr		
0.1 - 0.3 %	Fe, Zr		No	Zr
< 0.1 %	K, Mg, Si, Ca, Na	K, Ca, Fe, Mg, Si, Na	Ca, K, Mg, Na, Zr, Si	Ca, K, Mg, Na
Major Phase (Ceramic, SPS 1200C)	Rutile	Rutile		
Major Phase (Ceramic, SPS 1100C)	Rutile	Rutile		
Minor Phase (Ceramic, SPS1200C)	d=3.36A, unidentified	d=3.36A, unidentified		
Minor Phase (Ceramic, SPS1100C)	d=3.36A, unidentified	d=3.36A, unidentified		
Density (% Theoretical)				
SPS at 1200C	98.1	98.2		
SPS at 1100C	98.5	99.0		
Sintered Grain Size (μm)				
SPS at 1200C	~ 20	10 -20		
SPS at 1100C	~ 12	4 - 6		
Remark		Potassium spots found in SPS 1100C sample		

Table 8 Physical Properties of Powders Sintered by SPS

Sample	Composition	Sintering	Seebeck Coefficient (mV/K) Near 700C	Electrical Conductivity (S/cm) Near 700C	Power Factor (Watt/mK^2) Near 700C	Thermal Conductivity (Watt/mK) Near 700C	ZT Near 700C
00187K	0.97 TiO2 - 0.03 NbO2.5	SPS, 1100C	-330	3.20E+01	3.48E-04	3.70E+00	0.092
00187K	0.97 TiO2 - 0.03 NbO2.5	SPS, 1200C	-350	2.70E+01	3.31E-04	3.30E+00	0.098
00187L	0.97 TiO2 - 0.03 NbO2.5	SPS, 1100C	-370	2.40E+01	3.29E-04	3.30E+00	0.097
00187L	0.97 TiO2 - 0.03 NbO2.5	SPS, 1200C	-340	2.00E+01	2.31E-04	3.20E+00	0.070
00183K	1.0 SrO - 0.80 TiO2 - 0.20 NbO2.5	SPS, Condition 3	-130	2.00E+02	3.38E-04	3.87E+00	0.085
00183K	1.0 SrO - 0.80 TiO2 - 0.20 NbO2.5	SPS, Condition 1	-170	2.50E-01	7.23E-07	NT	< 0.01
00183L	1.0 SrO - 0.80 TiO2 - 0.20 NbO2.5	SPS, Condition 2	-145	1.10E+02	2.31E-04	4.50E+00	0.050
00183L	1.0 SrO - 0.80 TiO2 - 0.20 NbO2.5	SPS Condition 1	-210	1.60E-01	7.06E-07	NT	< 0.01
Company X Std.	proprietary	SPS Condition 1	-150	5.00E+02	1.13E-03	4.38E+00	0.250

Table 9 Thermoelectric Properties of Powders Sintered by SPS

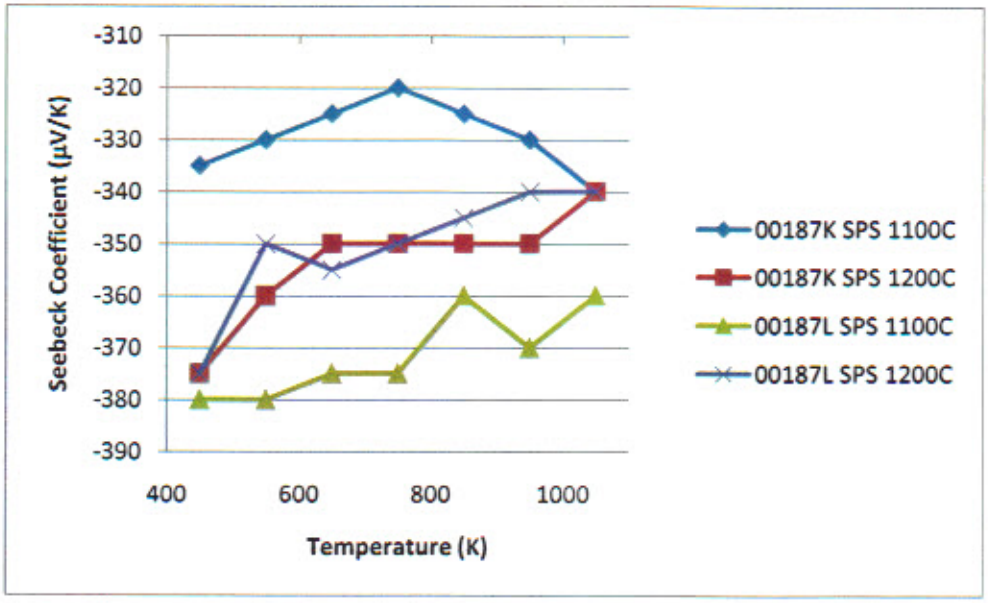

Fig. 6 Seebeck Coefficient of 0.97 TiO2 – 0.03 NbO2.5 vs. Temperature, Sintered by SPS

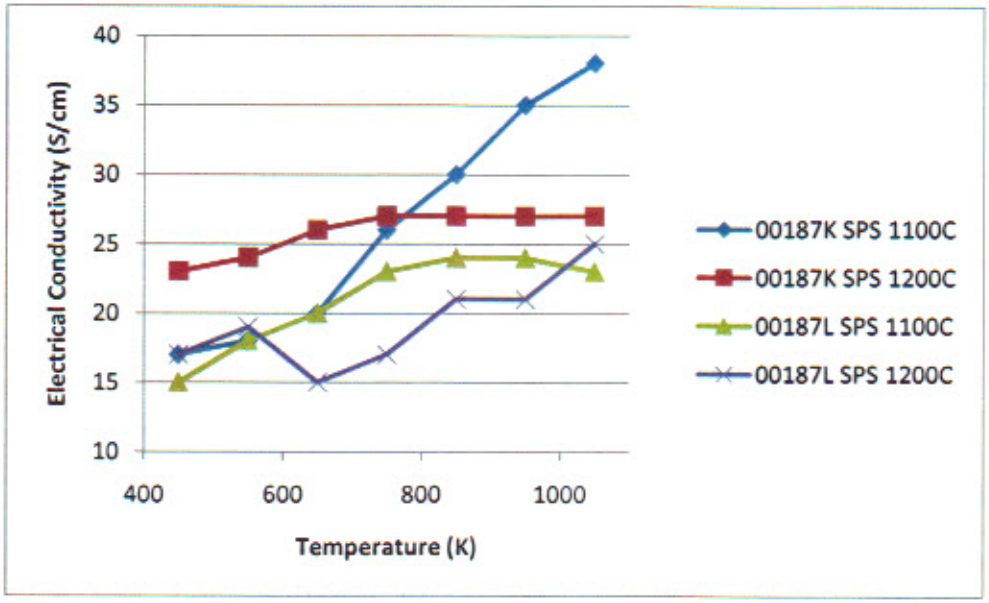

Fig. 7 Electrical Conductivity of 0.97 TiO2 – 0.03 NbO2.5 vs. Temperature, Sintered by SPS

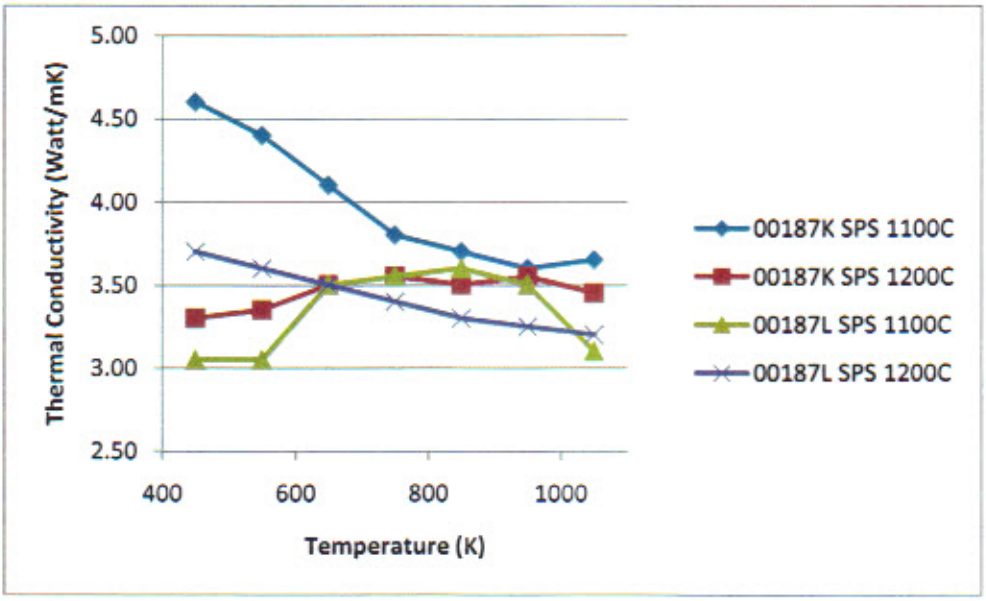

Fig. 8 Thermal Conductivity of 0.97 TiO2 – 0.03 NbO2.5 vs. Temperature, Sintered by SPS

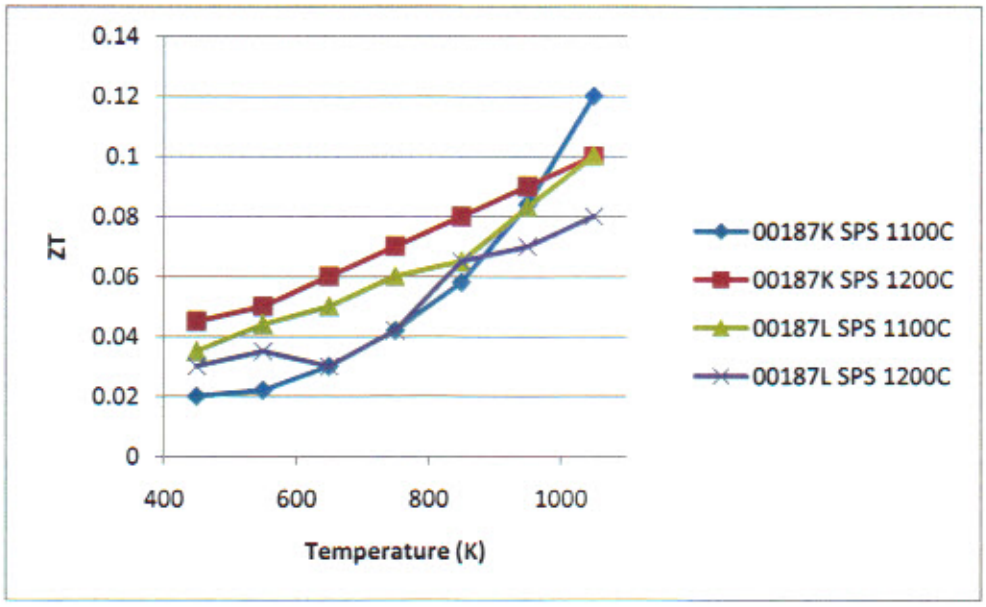

Fig. 9 ZT of 0.97 TiO2 – 0.03 NbO2.5 vs. Temperature, Sintered by SPS

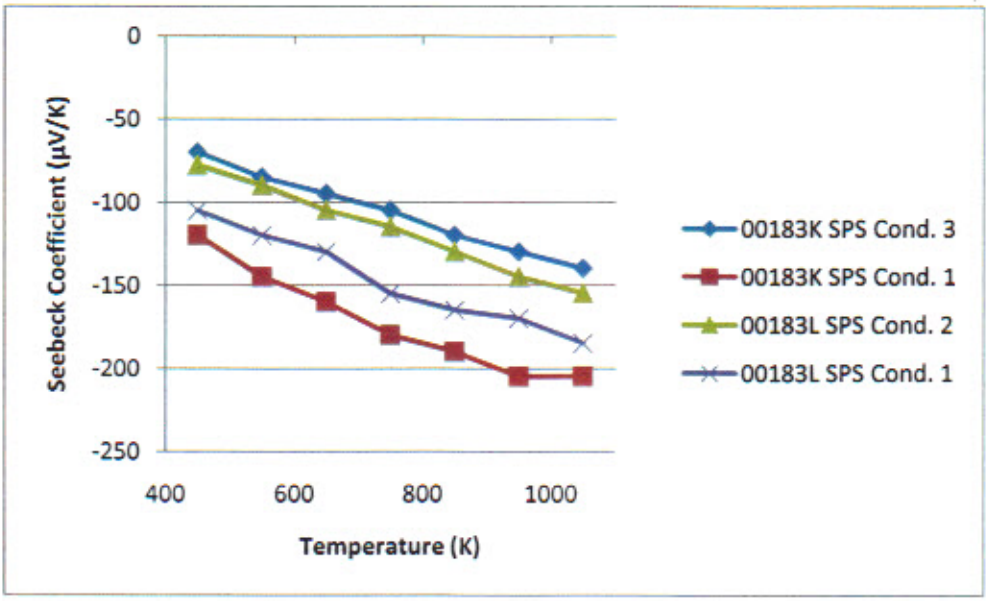

Fig. 10 Seebeck Coefficient of 1.0 SrO – 0.8 TiO2 – 0.2 NbO2.5 vs. Temperature, Sintered by SPS

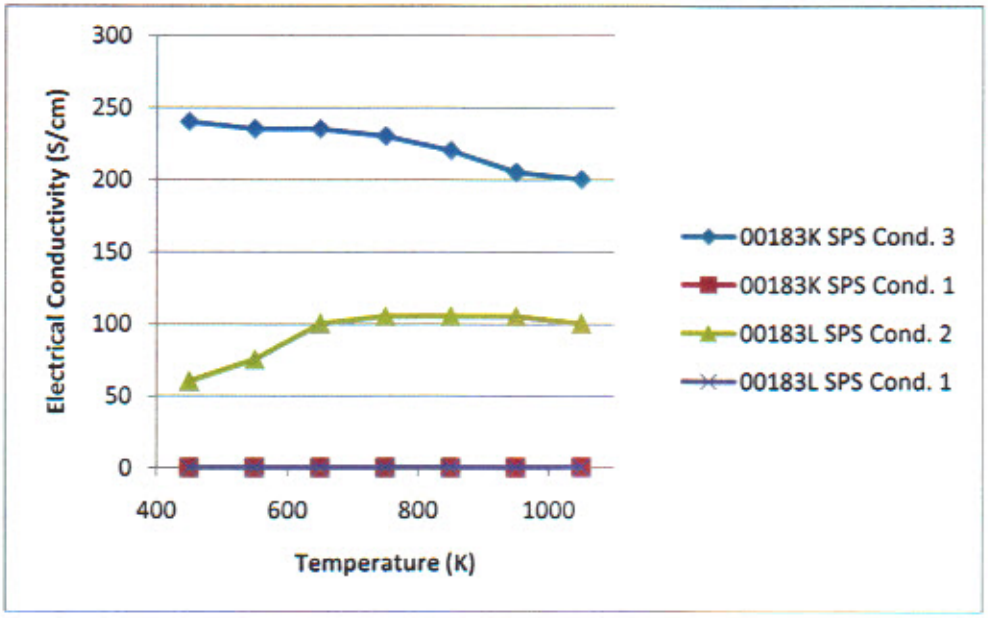

Fig. 11 Electrical Conductivity of 1.0 SrO – 0.8 TiO2 – 0.2 NbO2.5 vs. Temperature, Sintered by SPS

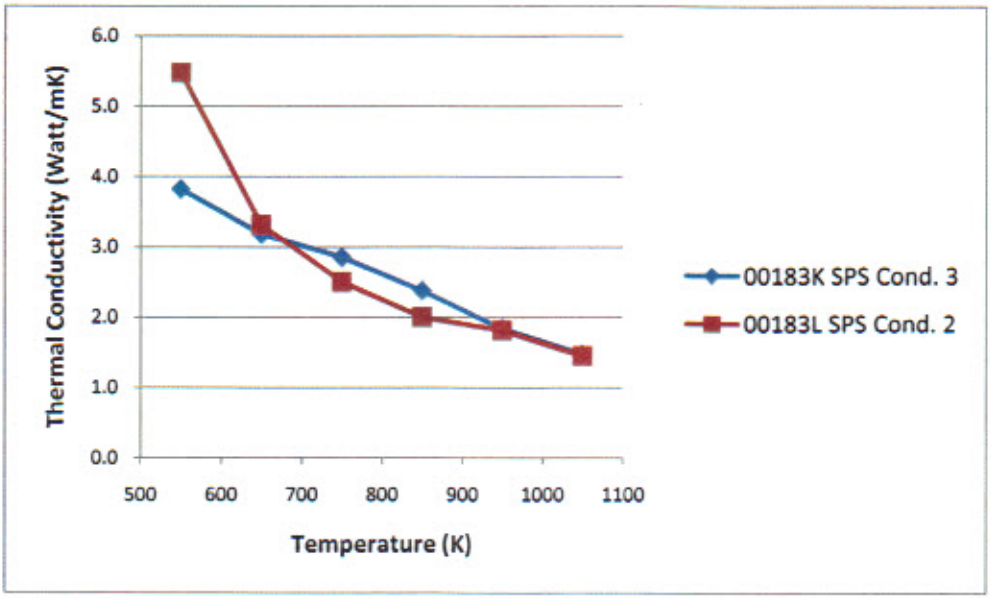

Fig. 12 Thermal Conductivity of 1.0 SrO – 0.8 TiO2 – 0.2 NbO2.5 vs. Temperature, Sintered by SPS

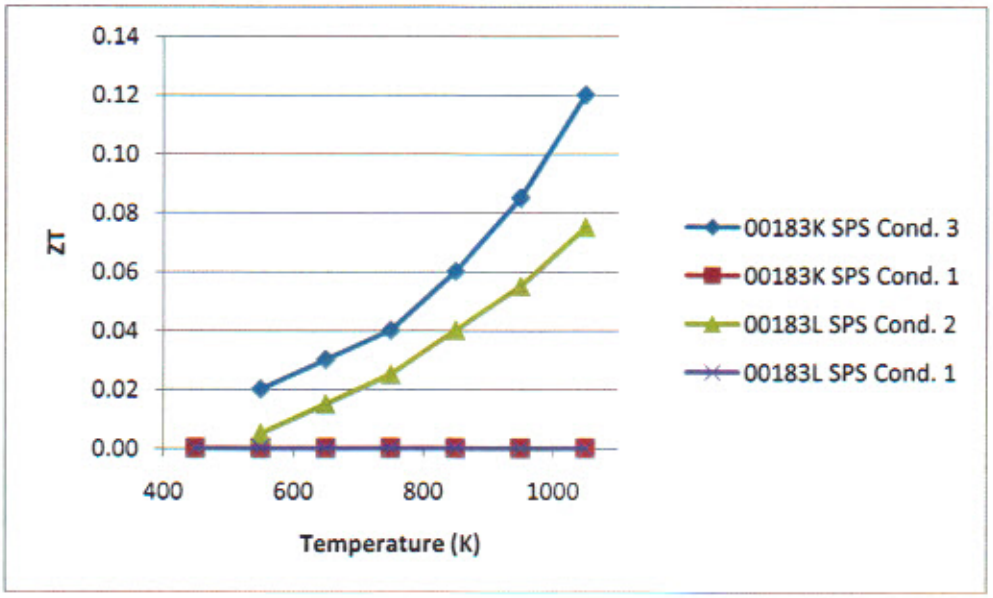

Fig. 13 ZT of 1.0 SrO – 0.8 TiO2 – 0.2 NbO2.5 vs. Temperature, Sintered by SPS

The above results of Company X's evaluation can be summarized into several major points.

1. With Company X's material processing and thermal testing expertise, both 0.97 TiO2 – 0.03 NbO2.5 and 1.0 SrO – 0.8 TiO2 – 0.2 NbO2.5 compositions show much improved thermoelectric properties. ZTs are approaching 0.1. The improvement is mainly due to the significant improvement of electrical conductivity. Notice that electrical conductivities from 100 S/cm to 500 S/cm were seen in samples with ZT > 0.05. It demonstrates again that electrical conductivity dictates largely the performance and ZT of the high temperature ceramic oxide thermoelectric materials.

2. The increase of electrical conductivity is largely attributed to Spark Plasma Sintering technology to sinter the ceramic. It was concluded that SPS is a MUST process for sintering high temperature ceramic oxide thermoelectric materials.

3. Seebeck coefficients of the two ceramic formulations chosen are not very sensitive to sintering conditions. Values of Seebeck coefficients of samples sintered by SPS are only slightly better than Seebeck coefficients of conventionally sintered samples regardless if the conventional sintering was done in air or in H2/Ar reducing atmosphere.

4. Both the 0.97 TiO2 – 0.03 NbO2.5 and the 1.0 SrO – 0.8 TiO2 – 0.2 NbO2.5 based compositions can be used as n-type precursor materials to develop more advanced and commercially scalable thermoelectric module design.

5. Company X made suggestions to reduce powder particle size to nano size by milling and to eliminate the minority phases by improving batching and/or calcine.

4.3 Task 4, Composition and Process Modification

Task 4 work actually started during Task 1 and Task 2 works. It was decided during the time to investigate the effect of powder particle size reduction by milling to see if electrical conductivity and thermoelectric properties could be improved. The milling was done with a commercial fine media milling equipment Mini-Por, manufactured by Netzsch (Exton, PA) using either 0.1 mm or 0.5 mm diameter yttria stabilized zirconia media. This equipment and technology will be referred to as Netzsch milling for the remaining of this report. Two compositions (0.97 TiO2 – 0.03 NbO2.5 and 1.0 SrO – 0.8 TiO2 – 0.2 NbO2.5) recommended by experts in the field were made and then submitted to the equipment company for Netzsch milling to reduce their particle size.

Table 10 shows physical and thermoelectric properties of Netzsch milled powders. Particle size data listed in Table 10 was measured by Microtrac-X100. It is noted that the 1.0 SrO – 0.8 TiO2 – 0.2 NbO2.5 powder Netzsch milled for 3 hours has much higher surface area than the 1 hour milled sample indicating that its particle size should be much smaller than the 1 hour Netzsch milled powder. However, actual particle size measurement by Microtrac-X100 showed its particle size was "coarser". It is believed that this is due to powder dispersion issue with Microtrac-X100 technique. Fig. 14, Fig. 15, and Fig. 16 show Seebeck coefficients, electrical conductivities, and ZT x thermal conductivity vs. temperature of the two Netzsch milled powders.

Material	0.97 TiO2 - 0.03 NbO2.5	0.97 TiO2 - 0.03 NbO2.5	1.0 SrO - 0.8 TiO2 - 0.2 NbO2.5	1.0 SrO - 0.8 TiO2 - 0.2 NbO2.5
Netzsch Milling Time (Hour)	1	3	1	3
D90 (μm)	1.05	0.81	0.96	0.60
D50 (μm)	0.71	0.60	0.69	0.94
D10 (μm)	0.52	0.48	0.53	1.34
SA (m2/g)	15.1	68.7	17.2	52.8
Sintered at 1450C/4H, Air				
Shrinkage (%)	15.8	20.6	16.8	No data due to
Apparent Density (g/cc)	4.10	3.80	4.99	disc cracked
Seebeck Coefficient (μV/K) at near 700C	-644	-464	-409	
Conductivity (S/cm) at near 700C	1.22E-02	5.77E-01	9.70E-03	
Power Factor (W/mK^2) at near 700C	5.06E-07	1.24E-05	1.62E-07	
ZTxThermal Conductivity (W/mK) at near 700C	4.92E-04	1.21E-02	1.58E-04	
Sintered at 1400C/4H, Air				
Shrinkage (%)	15.6	20.4	14.0	No data due to
Apparent Density (g/cc)	4.10	3.90	4.55	disc cracked
Seebeck Coefficient (μV/K) at near 700C	-70.5	-419	-235	
Conductivity (S/cm) at near 700C	5.47E-01	6.22E-01	3.05E-06	
Power Factor (W/mK^2) at near 700C	2.72E-07	1.09E-05	1.68E-11	
ZTxThermal Conductivity (W/mK) at near 700C	2.65E-04	1.06E-02	1.64E-08	

Table 10 Physical and Thermoelectric Properties of Netzsch Milled Thermoelectric Powders

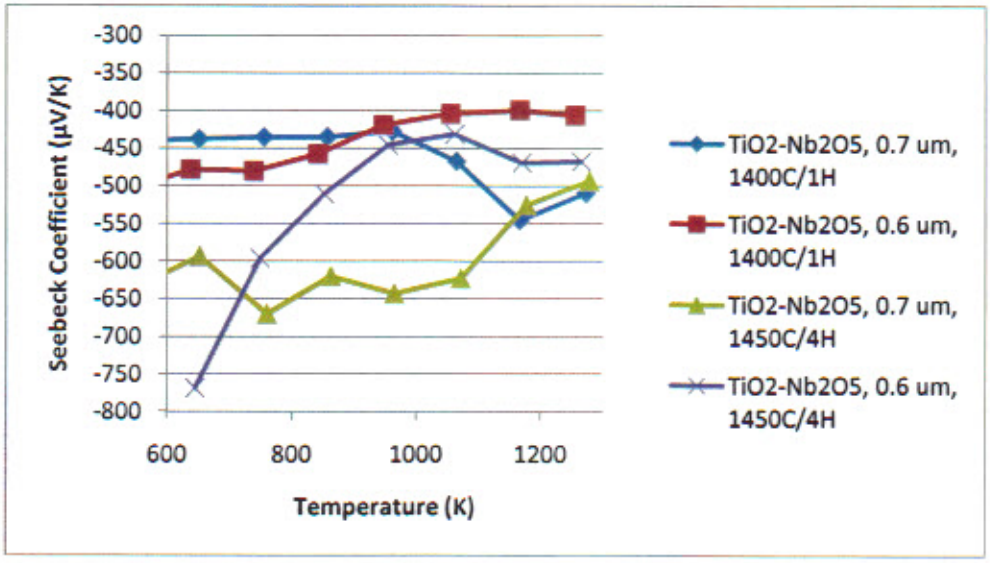

Fig. 14 Seebeck Coefficient vs. Temperature of Netzsch Milled 0.97 TiO2 – 0.03 NbO2.5 Powder

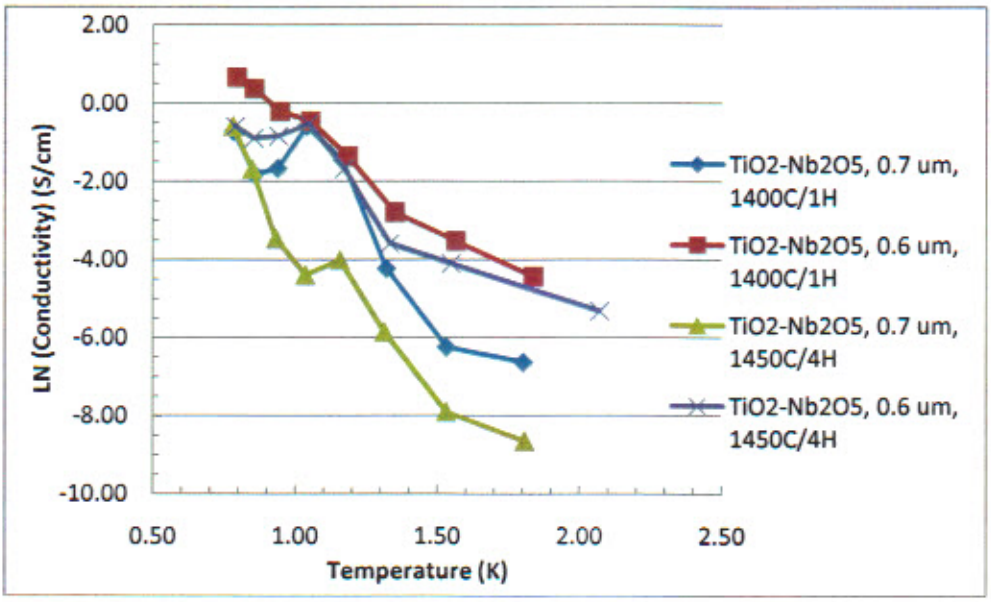

Fig. 15 Electrical Conductivity vs. Temperature of Netzsch Milled 0.97 TiO2 – 0.03 NbO2.5

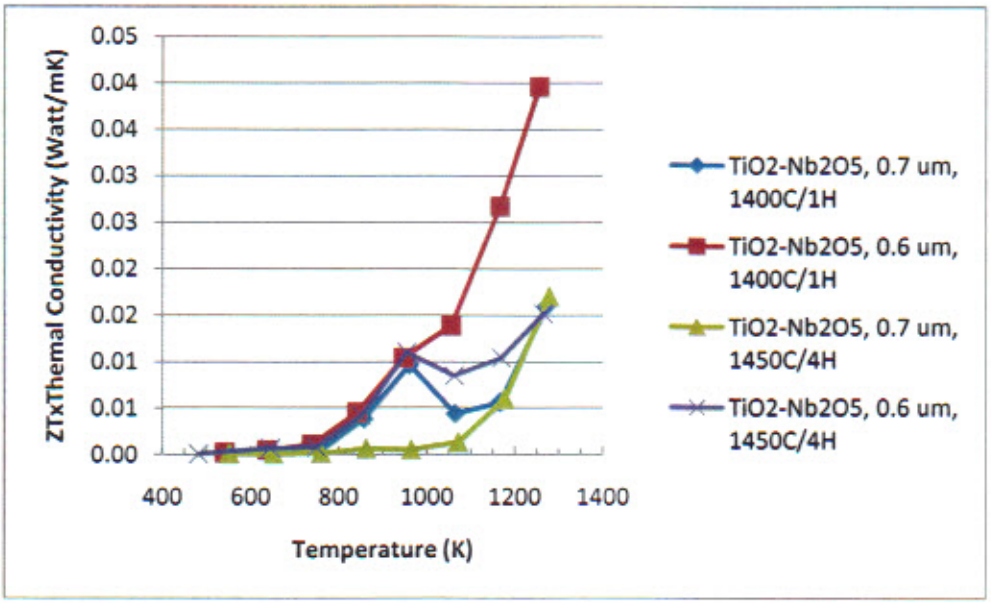

Fig. 16 ZT x Thermal Conductivity vs. Temperature of Netzsch Milled 0.97 TiO2 – 0.03 NbO2.5 Powder

It was encouraging to see that there was a case that some improvements were made by reducing the particle size of the powder. By Netzsch milling the 0.97 TiO2 – 0.03 NbO2.5 powder 3 hours instead of 1 hour, disc sintered at 1450°C in air had its electrical conductivity increased 50 times, power factor increased 25 times, and ZT x thermal conductivity increased 25 times. Although conductivity values are still very low for these samples due to discs sintered in air by conventional technique, it appears that reducing particle size of the powder has some benefits and is worth pursuing further. It also demonstrated again that electrical conductivity plays a critical role in obtaining high power factor and ZT. Thermoelectric data for 3 hours Netzsch

milled 1.0 SrO – 0.8 TiO2 – 0.2 NbO2.5 powder could not be obtained due to discs all cracked after sintering. There was not enough sample powder left to repeat the sintering and tests.

Follow Company X's recommendation after their first evaluation of micro meter size powders, two additional powders with much smaller particle sizes were made and evaluated. The composition of the first powder was 0.97 TiO2 – 0.03 NbO2.5 and the composition of the second powder was 1.0 SrO – 1.03x0.8 TiO2 – 1.03x0.2 NbO2.5. Note that the composition of the second powder was modified from the previous composition of 1.0 SrO – 0.8 TiO2 – 0.2 NbO2.5 by adding more B site ions of Ti and Nb but keeping Ti to Nb mole ratio the same. Past experience with dielectric materials based on perovskite ABO3 compounds such as BaTiO3, SrTiO3, CaTiO3 etc. was such that ABO3 materials with slight excess of B site ions usually have better sintering and densification behavior. Also, raw mix of the 1.0 SrO – 1.03x0.8 TiO2 – 1.03x0.2 NbO2.5 powder was Netzsch milled before calcine. These two powders were all Netzsch milled after calcine to nano particle size as indicated by high surface area of the powder after milling.

Company X evaluated these two nano size powders. The results for both powders are summarized in Table 11, Fig. 17 to Fig. 26.

Precursor Powder (Made by TAM)	1.00 SrO - 1.03x0.8 TiO2 - 1.03x0.2 NbO2.5		0.97 TiO2 - 0.03 NbO2.5	
Powder Surface Area (m2/g)	58.9		76.9	
Powder Size (nm)	< 50		20 – 30	
Major Phase	SrTiO3		TiO2	
Minor Phase	TiO2		NbO0.76, ZrO2	
Impurity	ZrO2, 6.8 wt%		ZrO2, 3.0 - 10.0 wt%	
Composition / Process Modification By Company X	Yes	Yes	No	Yes
Processing and Sintering	SPS, Condition A	SPS, Condition B	SPS1200C	SPS1200C
(At 700C)				
Electrical Conductivity (S/cm)	360	240	14	200
Seebeck Coefficient (μV/K)	-155	-152	-380	-130
Power Factor (Watt/mK^2)	8.65E-04	5.54E-04	1.60E-04	2.60E-04
Thermal Conductivity (Watt/mK)	3.6	3.6	2.6	3.1
ZT	0.23	0.15	0.06	0.09
Sintered Grain Size (μm)	~ 5	~ 5	Layered, ~ 4 and < 1	Layered, ~ 4 and < 1

Table 11 Physical and Thermoelectric Properties of Nano Size Powders, Sintered by SPS

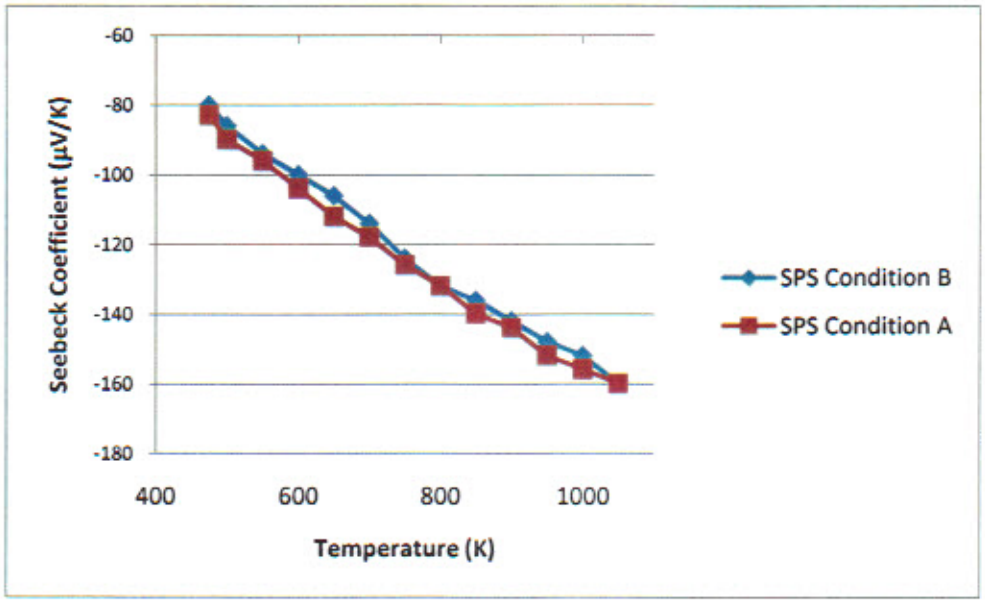

Fig. 17 Seebeck Coefficient vs. Temperature of Nano Size 1.0 SrO – 1.03x0.8 TiO2 – 1.03x0.2 NbO2.5 Powder

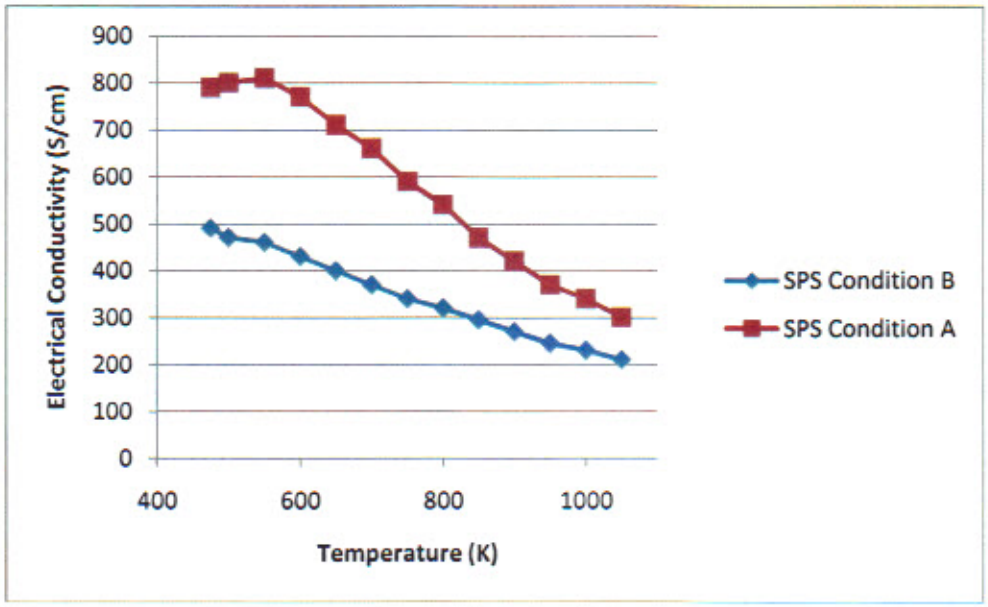

Fig. 18 Electrical Conductivity vs. Temperature of Nano Size 1.0 SrO – 1.03x0.8 TiO2 – 1.03x0.2 NbO2.5 Powder

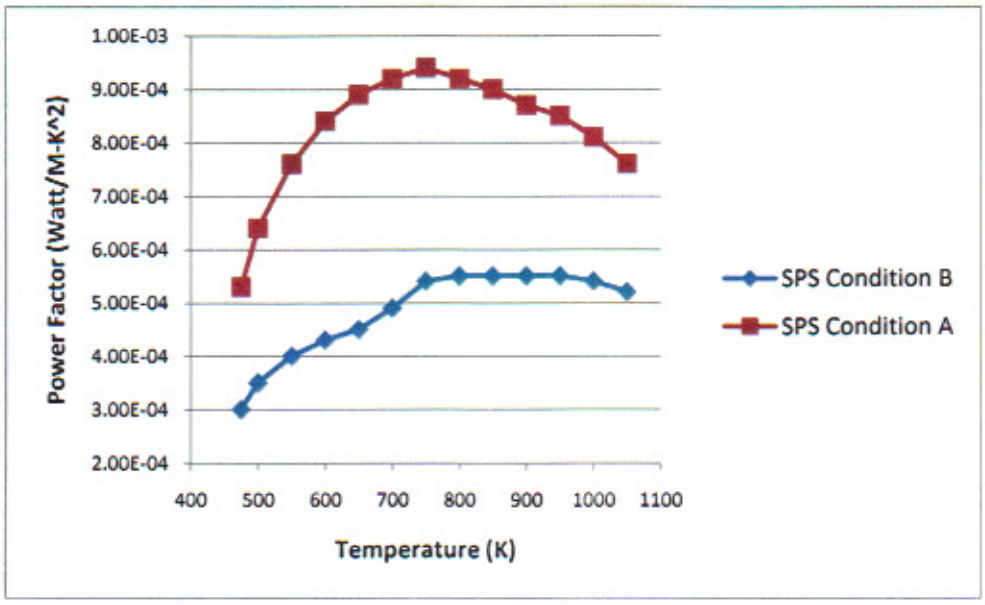

Fig. 19 Power Factor vs. Temperature of Nano Size 1.0 SrO – 1.03x0.8 TiO2 – 1.03x0.2 NbO2.5 Powder

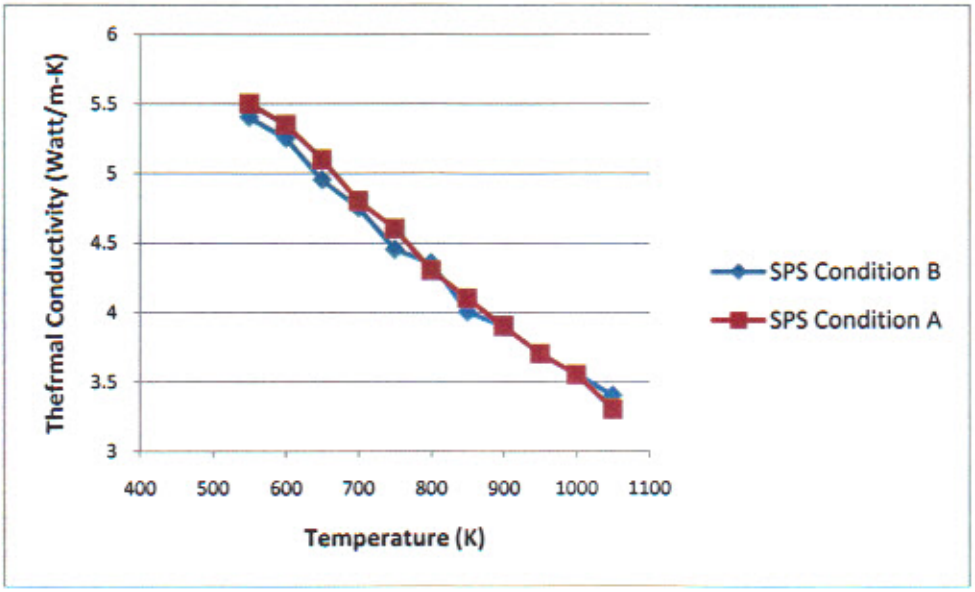

Fig. 20 Thermal Conductivity vs. Temperature of Nano Size 1.0 SrO – 1.03x0.8 TiO2 – 1.03x0.2 NbO2.5 Powder

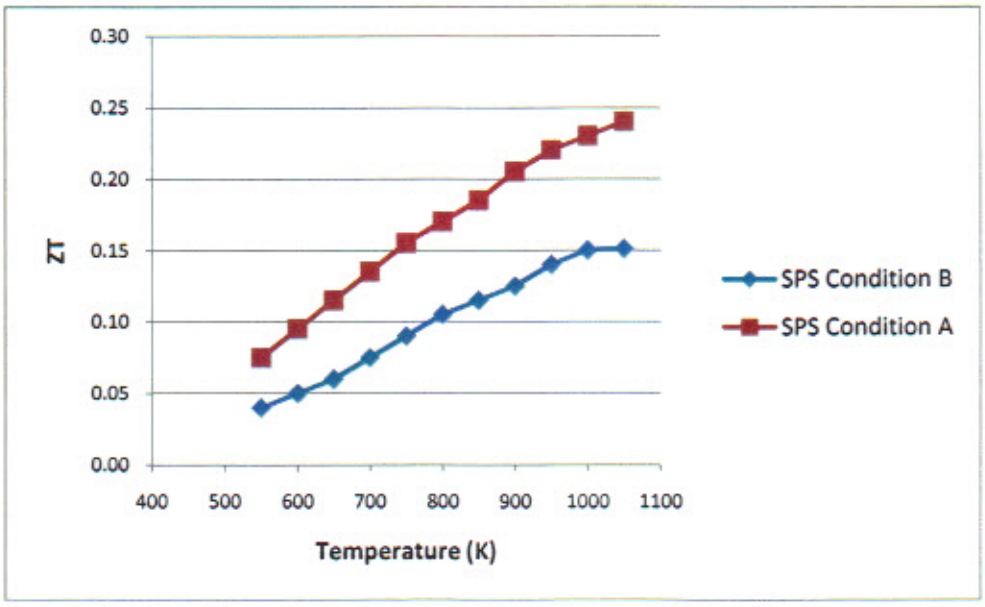

Fig. 21 ZT vs. Temperature of Nano Size 1.0 SrO – 1.03x0.8 TiO2 – 1.03x0.2 NbO2.5 Powder

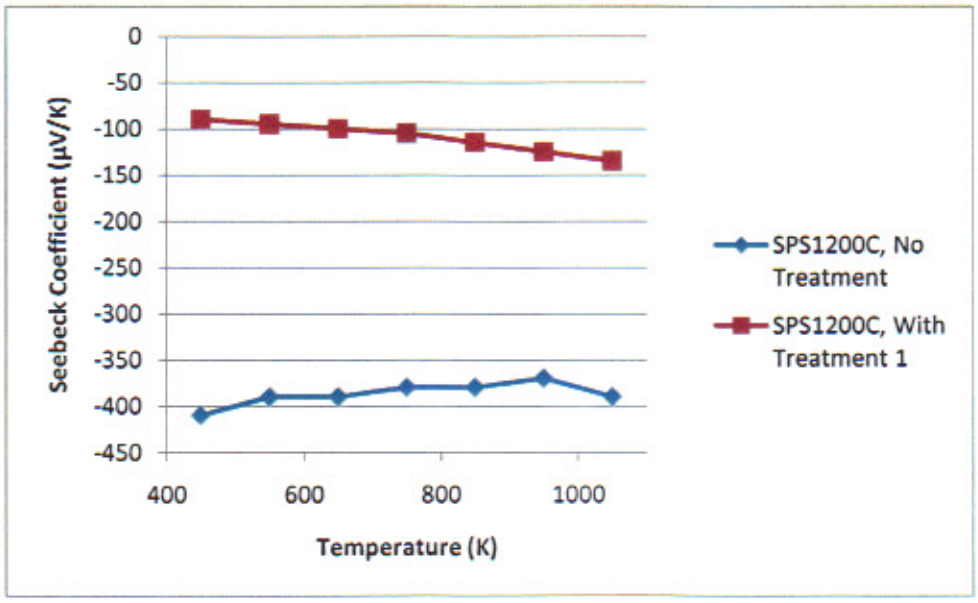

Fig. 22 Seebeck Coefficient vs. Temperature of Nano Size 0.97 TiO2 – 0.03 NbO2.5 Powder

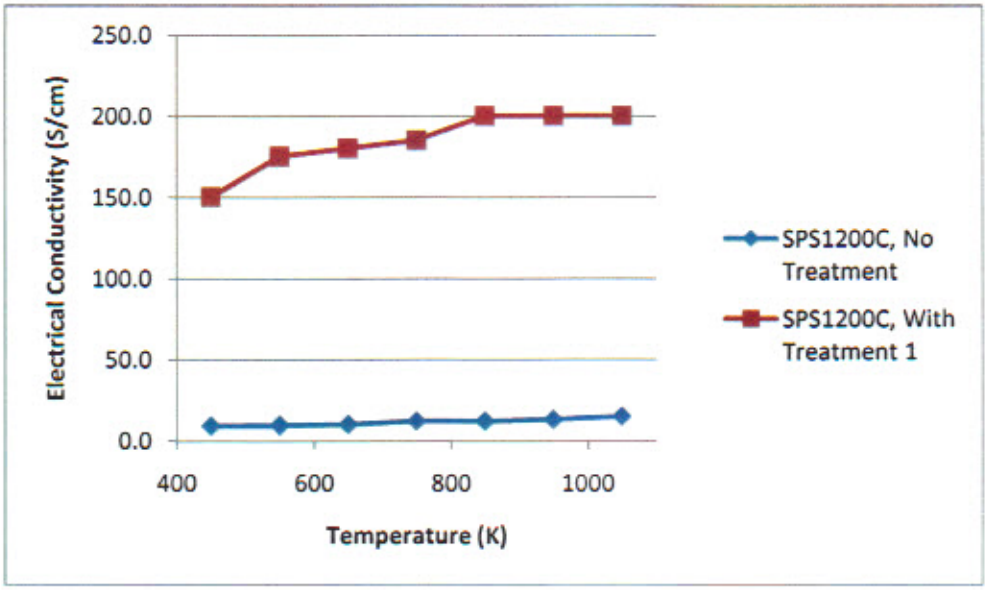

Fig. 23 Electrical Conductivity vs. Temperature of Nano Size 0.97 TiO2 – 0.03 NbO2.5 Powder

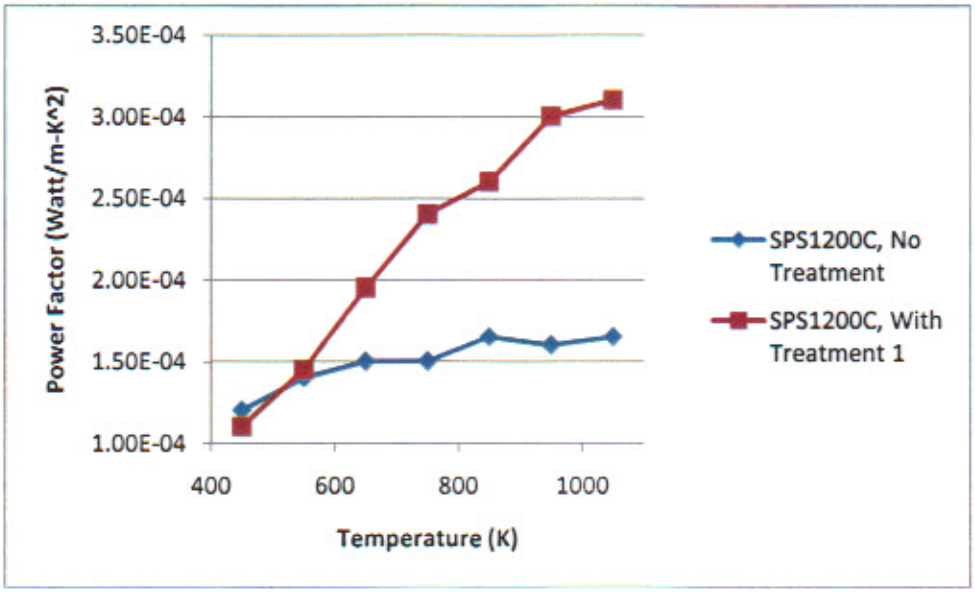

Fig. 24 Power Factor vs. Temperature of Nano Size 0.97 TiO2 – 0.03 NbO2.5 Powder

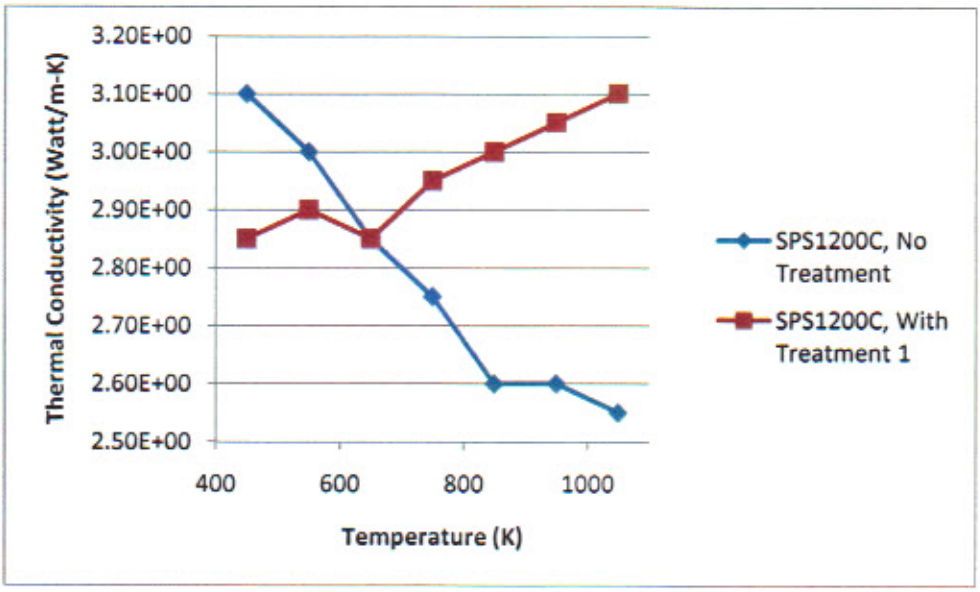

Fig. 25 Thermal Conductivity vs. Temperature of Nano Size 0.97 TiO2 – 0.03NbO2.5 Powder

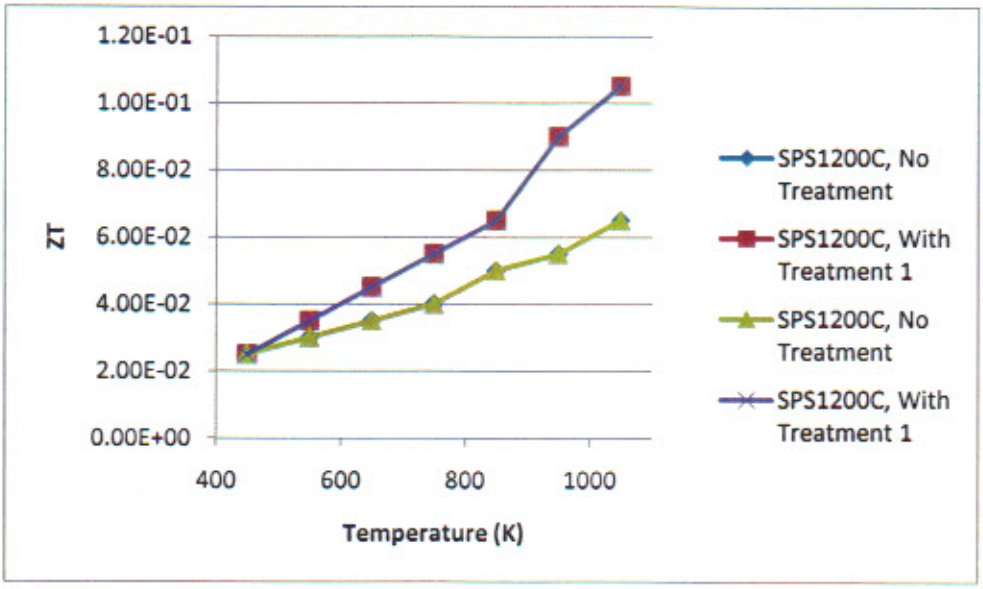

Fig.26 ZT vs. Temperature of Nano Size 0.97 TiO2 – 0.03 Nb2O5 Powder

As shown in the above Tables and Figures, the evaluation performed by Company X on the 1.0 SrO – 1.03x0.8 TiO2 – 1.03x0.2NbO2.5 and 0.97 TiO2 – 0.03 NbO2.5 powders shows several very encouraging results;

A) For 1.0 SrO – 1.03x0.8 TiO2 – 1.03x0.2 NbO2.5 composition

By Netzsch milling the raw mix and/or slightly increase the (Ti+Nb)/Sr mole ratio, Calcination was more complete and phase pure powder could be obtained. The Sr5Nb4O15 and SrNb4O6

phases as detected in the earlier 1.0 SrO – 0.8 TiO2 – 0.2 NbO2.5 powder samples were not detected.

Electrical conductivities of nano size powders processed at both SPS condition A and SPS condition B were increased to 360 S/cm and 240 S/cm. With only one exception, they are significantly higher than previous micro size 1.0 SrO – 0.8 TiO2- 0.2 NbO2.5 powders processed at SPS Conditions 1, 2 and 3 (0.16 to 200 S/cm). [Table 11, Table 9]

Seebeck coefficients of nano size powders processed under SPS conditions A and B (-155 μV/K, -152 μV/K) were comparable to previous 1.0 SrO – 0.8 TiO2 – 0.2 NbO2.5 samples processed under SPS conditions 1, 2 and 3. (-170 μV/K, -210 μV/K, -145 μV/K, and -130 μV/K) [Table 11, Table 9]

The overall effect was that ZT was increased from 0.05 – 0.085 to 0.15 – 0.25.

It demonstrated that, with proper SPS conditions and/or slight modification of composition, the SrO – TiO2 – NbO2.5 composition system shows good thermoelectric properties to begin with and can be used as base n-type material for integrated TE module design.

It is interesting to note that, after Company X processed, the 1.0 SrO – 1.03x0.8 TiO2 – 1.03x0.2 NbO2.5 composition had its electrical conductivity decreased as the temperature was increased (Fig. 18). It indicates a metallic type electrical conduction behavior. It is suspected that Company X added a small amount of high electrical conductive phase to the 1.0 SrO – 1.03x0.8 TiO2 – 1.03x0.2 NbO2.5 base powder to increase significantly its electrical conductivity.

B) For 0.97 TiO2 – 0.03 NbO2.5 composition

There was not much change with phase purity of nano size powder as compared with earlier micro size powder. Thermoelectric properties were also comparable between nano size and micro size powders. [Table 11, Table 9]. The electrical conductivity could be improved significantly when Company X applied their proprietary composition and/or processing modifications to the precursor material. However, improvement of ZT was less because Seebeck coefficient went down at the same time.

For this 0.97 TiO2 – 0.03 NbO2.5 composition system the electrical conductivity increased slightly with temperature at temperatures below 600°K and remains nearly constant at higher temperatures above 600°K.

4.4 Task 5, Design of Commercial Prototype

For Task 5, a preliminary design and optimization of a thermoelectric generator (TEG) that uses the n-type SrTi(0.8)Nb(0.2)O3 based ceramic material was performed. This modeling and optimization exercise allows one to estimate how practical physically, technically, and economically to fit chosen thermoelectric materials into an actual module to generate renewed usable energy. This work was performed by Dr. Brian T. Helenbrook at Clarkson University (Potsdam, New York) as a consultant under this project.

The design and optimization involved modeling exhaust heat exchange (EHX), TEG, and coolant heat exchange (CHX) as a whole system. The TEG module utilized engine exhaust gases for the hot source and coolant as cold source. The engine was chosen to be that of one used in a light

duty pick-up truck. The coolant was chosen to be the standard automobile antifreeze coolant. The composition of 1.0 SrO – 1.03x0.8 TiO2 – 1.03x0.2 NbO2.5 as discussed in Task 4 work was chosen as the n-type thermoelectric leg. Physical and thermoelectric properties of this material as shown in Table 10, Figure 17, 18, 19, 20, and 21 in previous sections were chosen as design inputs. As a candidate p-type material has yet to be developed, it was assumed that the p-type legs have properties similar to n-type legs. Since the ceramic thermoelectric materials can withstand higher temperatures than most thermoelectric materials, the TEG was placed immediately after the exhaust manifold.

The optimization results as given in Table 1 of Dr. Helenbrook's report showed that the 1.0 SrO – 1.03x0.8 TiO2 – 1.03x0.2 NbO2.5 thermoelectric material as it stands now does not offer significant opportunity for energy saving when fabricated into a TEG device. Even though the TEG can produce 124 W output (216 W effective shaft power), only 2.4 W net shaft power (< 10% of the TEG output) could be available as renewed energy for use. Most of the power generated by the TEG had to be consumed on exhaust, coolant, and transport system to accommodate the installation of TEG. This design suffers mainly because of the high thermal conductivity of the thermoelectric material. The mass of the TEG was calculated to be heavy as 35 kg. Also because of the high thermal conductivity, long thermoelectric legs would be required. This made the device width fairly large and unwieldy as the report said. The modeling and optimization was repeated with the assumption that thermal conductivity of the thermoelectric material was reduced by a factor of 2. The results as given in Table 2 of Helenbrook's report were much better. TEG can now produce 264 W power output (465 W effective shaft power). 216 W net shaft power (> 45%) can be available as renewed energy for use. Also, length of the thermoelectric legs could be reduced by half.

The above modeling and optimization technique is a very useful tool in estimating; (a) how practical physically, technically, and economically to fit chosen thermoelectric materials into an actual module to generate renewed usable energy, (b) optimum design of the TEG device, (c) material consumption of the TEG device, and (d) material and manufacturing cost of the TEG device.

Dr. Brian Helenbrook's report is attached in the following

TEG Generator Optimization

B. T. Helenbrook
Clarkson University

1 Thermoelectric Generator

In this section, a preliminary design of a thermoelectric generator (TEG) that uses the n-type $SrTi(0.8)Nb(0.2)O_3$ ceramic material is given. The TEG is designed to utilize engine exhaust gases for the hot source. As the ceramic material can withstand higher temperatures than most thermoelectric materials, it was decided to place the TEG immediately after the exhaust manifold. The exhaust characteristics were chosen to be that of an engine used in a light-duty pick-up truck, a 5.3 liter V8 gasoline engine. The engine has a nominal rating of 200 kW at 5000 rpm and 430 N m of torque at 4000 rpm. The exhaust stream exiting the manifold from this engine was taken as $\dot{m}_e = 0.049$ kg/s at a temperature of 670C where $\dot{m}_e$ is the mass flow rate of the exhaust. These conditions are typical of what would be expected for a vehicle traveling at 70 mph [1-3].

1.1 Basic Design

The basic design of the generator is a counterflow heat exchanger sandwich type as shown in Figure 1. The center of the device is the hot gas heat exchanger. This is surrounded on either side by the thermoelectric legs, which are in turn surrounded by the coolant heat exchangers. For the exhaust gas heat exchanger, an offset strip fin type arrangement is used such as that shown in Figure 2. For the coolant side heat exchanger a series of rectangular flow channels is used such as that shown in Figure 3. These devices will be manufactured out of a lightweight highly conductive material such as Corning glass.

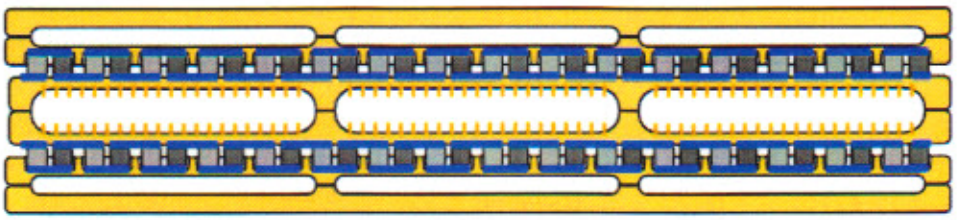

Figure 1: Schematic of the thermoelectric generator design

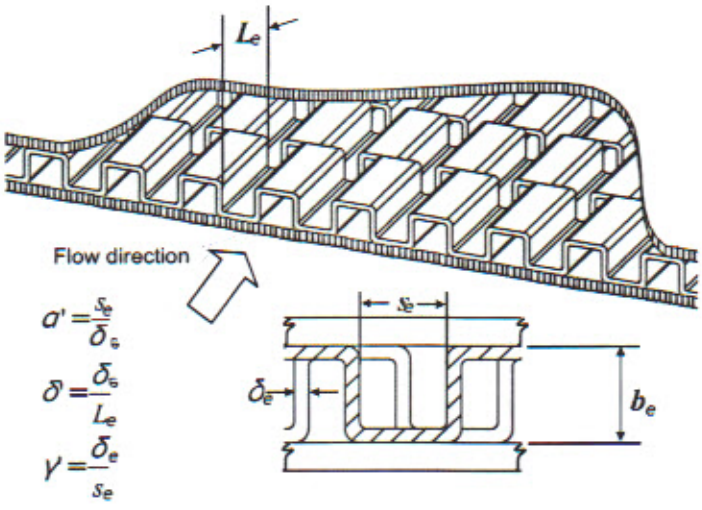

Figure 2: Strip fin exhaust heat exchanger

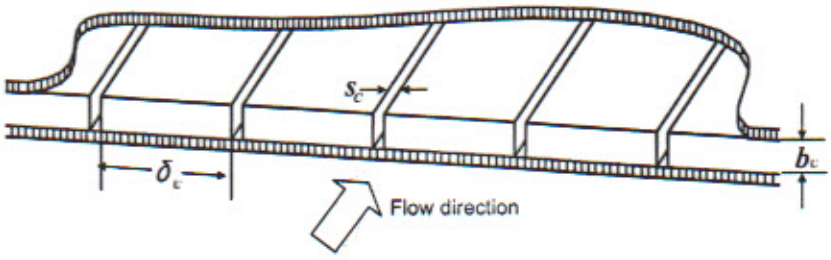

Figure 3: Coolant heat exchanger

Clearly even the heat exchangers have a large design space associated with them. The hot gas heat exchanger has four design parameters as shown in the figure, L_e, s_e, b_e, and δ_e. These can be determined from the three geometric ratios a', δ' and γ' and one length scale. For this optimization study, the three geometric ratios were fixed and only the scale of the heat exchanger was varied. The geometric ratios were given by a'=0.38, δ'=0.06, and γ'=0.38. These values were chosen on designs tested in Kays and London [4].

For the coolant side, the design parameters, s_c, δ_c, and b_c, shown in Figure 3, were all fixed based on the heat exchanger used for automobile exhaust thermoelectric generation in [1]. The values used were $\delta_c = 23mm$, $s_c = 4mm$, and $b_c = 12.7mm$. On the coolant side, only the coolant mass flow rate was used as a design variable. In a typical installation, the coolant lines would tap into the main system on either side of the heater core. The mass flow rate can then be controlled by changing the resistance of the coolant loop, either with values or by appropriately choosing the flow resistance of the coolant inlet lines.

For the generator, the p- and n-type thermoelectric legs were assumed to be connected electrically in series. The material properties of the n-type legs were those measured in the preceding sections. As a candidate p-type material has yet to be developed, we assumed that the p-type legs have similar properties. Each leg was assumed to have a uniform cross section. The main design parameters for the legs are the cross-sectional area of the legs and the length of the thermoelectric legs. The actual design variables used are the couple density, ζ, which has units of number of legs per area and the aspect ratio of the legs, γ, which is the length of the legs divided by their cross-sectional area.

1.2 Modeling

The performance of the system is predicted using 1D models. Many of the modeling details can be found in [5]. The basic energy flow pathways are shown in Figure 4, which is a schematic of a finite cross-sectional area of the generator. To model the thermal section j shown in Figure 4, it is assumed the axial conduction in the metal is negligible and that the junction temperatures: $T_{h,j}$ and $T_{c,j}$, are uniform over the discretization area, A.

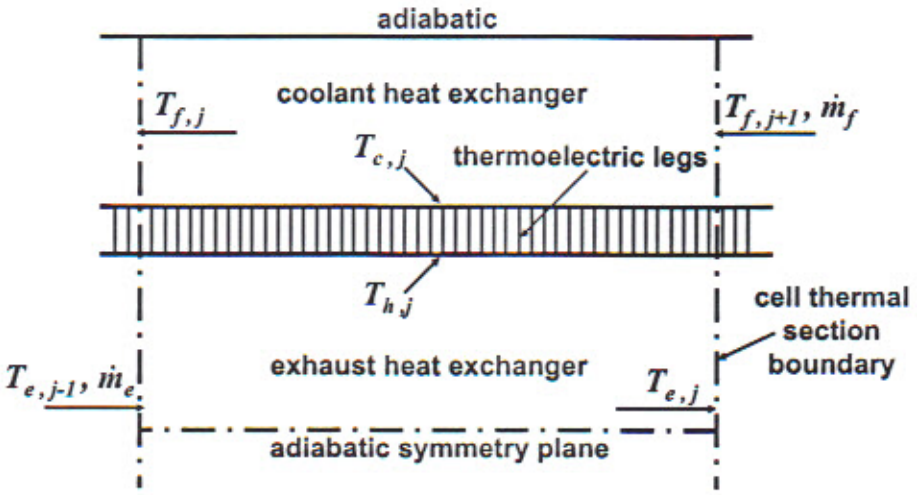

Figure 4: Side view of a thermal section.

A steady-state energy balance on the coolant heat exchanger (CHX) section considering convection in the fluid and conduction heat transfer to the module surface gives,

$$c_{p_{f,j}} T_{f,j} - c_{p_{f,j+1}} T_{f,j+1} - \frac{\overline{U}_{f,j} A}{\dot{m}_f} \left(T_{c,j} - \overline{T}_{f,j} \right) = 0, \tag{1}$$

where $\overline{U}_{f,j}$ is the average overall heat transfer coefficient for the CHX for this section, $\dot{m}_f$ is the mass flow rate of the coolant through the section, $c_{p_{f,j}}$ and $c_{p_{f,j+1}}$ are the specific heat of the coolant evaluated at $T_{f,j}$ and $T_{f,j+1}$, $T_{c,j}$ is the uniform cold junction temperature of the module j, and $\overline{T}_{f,j}$ is the average bulk temperature of the coolant for this section. $\overline{T}_{f,j}$ is defined as,

$$\overline{T}_{f,j} = \frac{1}{2} \left(T_{f,j} + T_{f,j+1} \right) \tag{2}$$

Similarly, for the EHX segment,

$$c_{p_{e,j}} T_{e,j} - c_{p_{e,j-1}} T_{e,j-1} - \frac{\overline{U}_{e,j} A}{\dot{m}_e} \left(\overline{T}_{e,j} - T_{h,j} \right) = 0, \tag{3}$$

where the variables have definitions similar to those in equation (1).

Balancing the energy flow in and out of the module gives,

$$\overline{U}_{e,j}A\left(\overline{T}_{e,j}-T_{h,j}\right)-\overline{U}_{f,j}A\left(T_{c,j}-\overline{T}_{f,j}\right)-P_j=0. \tag{4}$$

where P_j is the power generated by the legs in the discretization area,

$$P_j=IV_j=I(V_{oc,j}-IR_j). \tag{5}$$

I is the total current of the generator, $V_{oc,j}$ is the module's open circuit voltage, and R_j is the electrical resistance of the discretization area,

$$R_j=N_{c,j}\gamma\left(\overline{\rho}_n+\overline{\rho}_p\right) \tag{6}$$

where $N_{c,j}$ is the number of (series-connected) couples in the discretization area. The aspect ratio of the legs (γ) is assumed uniform over the generator. The number of couples in the discretization area, $N_{c,j}$, is given by

$$N_{c,j}=\zeta A, \tag{7}$$

where ζ is again the couple density.

The module's open circuit voltage, $V_{oc,j}$, is defined as,

$$V_{oc,j}=\alpha_j\left(T_{h,j}-T_{c,j}\right) \tag{8}$$

where α_j is the effective Seebeck coefficient of the discretization area. α_j is defined as:

$$\alpha_j=N_{c,j}\left(\overline{\alpha}_p-\overline{\alpha}_n\right). \tag{9}$$

and the total current of the generator, I, is defined as,

$$I = \frac{V_{oc}}{R_g + R_L} = \frac{\sum_{j=1}^{N_m} V_{oc,j}}{\sum_{j=1}^{N_m} R_j + R_L}, \tag{10}$$

where V_{oc} is the total open circuit voltage of the generator, R_g is the total electrical resistance of the generator, R_L is the load resistance.

A heat balance at the hot junction of the module as derived in [6] is,

$$\overline{U}_{e,j} A\left(\overline{T}_{e,j} - T_{h,j}\right) - K_j\left(T_{h,j} - T_{c,j}\right) - \alpha_j T_{h,j} I + \frac{1}{2} I^2 R_j = 0, \tag{11}$$

where K_j is the thermal conductance of the legs. K_j is defined as,

$$K_j = \frac{N_{c,j}}{\gamma}\left(\bar{k}_n + \bar{k}_p\right) \tag{12}$$

Finally, the power of the entire generator is,

$$P_g = I^2 R_L. \tag{13}$$

For the optimization of the system, it is also required to know the parasitic losses incurred by the TEG system. These consist of blow-down work because of the additional exhaust back pressure caused by the exhaust heat exhanger, the additional coolant pumping power, and for mobile applications the additional rolling resistance caused by the weight of the TEG. Both the exhaust blow down work, ΔP_e, and the coolant pumping parasitic powers, ΔP_p are estimated using the following expression

$$\Delta P = \frac{\rho Q^3 k}{\eta} \tag{14}$$

where k is a pressure loss coefficient for the heat exchanger, Q is the volumetric flow through the heat exchanger, and ρ is the density of the fluid (coolant or exhaust gas). These power are converted to a shaft

power using the efficiency η. For the coolant, η is the efficiency of the coolant pump, which was taken as 0.66. The exhaust pumping efficiency is the ratio of the change in shaft power caused by a change in exhaust pumping work. We have assumed a value of 0.8 which is what one could easily attain by using a blower to overcome the additional back pressure.

For mobile applications, the parasitic power to transport the total weight of the TEG system is given by

$$\Delta P_D = \frac{\mu_D W_T v}{\eta_D}, \tag{15}$$

where μ_D is the rolling resistance coefficient, W_T is the weight of the TEG system, v is the velocity of the vehicle, and η_D is the driveline transmission efficiency. The driveline transmission efficiency accounts for the losses in the linkages between the drive shaft and the wheels and is a function of vehicle speed. The weight of the system is estimated using the solid volume of the heat exchangers assuming they are constructed from a lightweight conductive material, Corning Glass substrate, having a density of 2230 kg/m^3.

To complete the entire system, auxiliary relations for the heat transfer coefficients and pressure loss coefficients must be supplied. The details of these relations are given in [5]. The entire generator is discretized as discussed above and the resulting coupled system of equations is solved using a Newton-Raphson iteration. This then predicts the power output of the TEG. For the purposes of optimization, the electrical output of the generator is converted to shaft power by multiplying by the power-conditioning unit efficiency and dividing by the alternator efficiency because the electrical power supplied by the TEG reduces the amount of shaftpower required for the alternator. The objective function for optimization is the sum of this TEG shaft power minus the parasitic shaft powers.

2 Optimization Results

In addition to the above discussed design parameters, one must also choose the length and width of the generator, L_x and L_y, where the

length is measured in the direction of the flow. The design parameters for the study are then

- coolant mass flow rate, $\dot{m}_c$
- exhaust gas heat exchanger size, b_e
- couple density, ζ
- couple aspect ratio, γ
- length of generator in streamwise direction, L_x
- length of generator in cross-stream direction, L_y

As the size of the device will be constrained by the available space in the vehicle engine compartment, we study the response to L_x and L_y parametrically rather than letting the optimizer automatically find the optimum size of the generator. An additional simplification in the design space is that the two design parameters γ and ζ always appear as the product γ/ζ in the one-dimensional model. Thus, this product is used as a single design variable. The product of γ/ζ is essentially the length of the legs. The area of the legs is not critical because it is assumed in the 1D model that all of the heat passes through the legs and there is no parasitic heat transfer between the legs.

To investigate different size generators, a 3x3 matrix of L_x and L_y variables was investigated given by ([0.5, 0.75, 1.0]m × [0.5, 0.75, 1.0]m). These were chosen as potentially reasonable sizes for a TEG. Although the 1D analysis treats all of the components as planar, there is no reason that the flow paths have to be strictly recti-linear. A more compact device could be made by serpentining the flow path. Table 1 shows the optimized results for $L_x, L_y = 0.5, 0.5m$.

$\dot{m}_c$	b_e	γ/ζ (m)	P_g (W)	ΔP_e (W)	ΔP_p (W)	ΔP_w (W)	*Net* (W)
0.17	0.022	0.15	124 (216)	33	36	144	2.4

Table 1: Optimal design results for the thermoelectric generator using the $SrTi(0.8)Nb(0.2)O_3$ ceramic material with $L_x = L_y = 0.5\ m$

The TEG generates 124 Watts of power, but the net reduction in shaft power caused by the TEG is only 2.4W. (The number in

parenthesis is the effective shaft power of the TEG). The net change in shaft power is small primarily because the thermal conductivity of the material is high and thus the efficiency of the thermoelectric material (ZT) is low. The power generated just barely offsets the parasitic powers of which the weight penalty is the largest. The mass of the generator was calculated to be 35 kg and the rolling resistance of the vehicle was 0.012. This weight penalty significantly reduces the benefit of the TEG for mobile applications.

Another outcome of the high thermal conductivity of the thermoelectric material is that long thermoelectric legs are required. The optimal length of the thermoelectric legs basically is a result of matching thermal resistance between the heat exchangers and the thermoelectric legs. Because the thermal conductivity of the material is high, long legs are required to create enough thermal resistance to maintain a significant temperature difference across the legs. This makes the device width fairly large and unwieldy. As we anticipate that the thermal conductivity of the material will be significantly reduced by the particle size reduction and SPS sintering process, we have run another optimization using one half the thermal conductivity. The results are shown in Table 2. Because of the lower thermal conductivity of the legs, shorter legs are needed and a greater conversion efficiency is attained. In this case, the device produces 216 W at the shaft.

$\dot{m}_c$	b_e	γ/ζ (m)	P_g (W)	ΔP_e (W)	ΔP_p (W)	ΔP_w (W)	*Net (W)*
0.21	0.021	0.06	264 (465)	64	39	144	216

Table 2: Optimal design results for the thermoelectric generator using the $SrTi(0.8)Nb(0.2)O_3$ ceramic material with decreased thermal conductivity and $L_x = L_y = 0.5\ m$

The amount of power produced depends on the area chosen for the generator. If an area of $1 \times 1 m^2$ is used a net electrical power of 415 W can be generated. However this is offset by the increased weight of the

device so the net shaft power actually decreases. If we optimize including L_x and L_y using a constraint that the maximum size in either direction not exceed 1 m, the optimum size for the generator is $L_x = 0.3m$ and $L_y = 1\text{m}$ which generates 316 Watts of electrical power and 276 Watts of net shaft power. For mobile applications, the weight penalty is the dominant loss mechanism. If one were to design for a stationary application, the optimum size of the generator and the corresponding output power would be significantly greater.

References

[1] M. A. Karri, Modeling of an automotive exhaust thermoelectric generator, Master's thesis, Clarkson University, Department of Mechanical and Aeronautical Engineering, Potsdam, NY (2005).

[2] M. A. Karri, B. T. Helenbrook, E. F. Thacher, Exhaust energy conversion by thermoelectric generation: Two case studies, accepted to Energy Conversion and Management .

[3] E. F. Thacher, B. T. Helenbrook, M. A. Karri, C. J. Richter, Testing an automobile exhaust thermoelectric generator in a light truck, Proc. IMechE, Part D: J. Automobile Engineering 221 (D1) (2007) 95–107.

[4] M. W. Kays, A. L. London, Compact Heat Exchangers, 3rd Edition, Krieger Publishing Co., 1998.

[5] M. A. Karri, Modeling and optimization of exhaust thermoelectric generator, Ph.D. thesis, Clarkson University, Department of Mechanical and Aeronautical Engineering, Potsdam, NY (2010).

[6] S. W. Angrist, Direct Energy Conversion, Allyn and Bacon Inc., Boston, MA, USA, 1971.

5.0 CONCLUSIONS

Most of the ceramic compositions selected for Phase I study have reasonable values of Seebeck coefficients. However, when sintered by conventional method, their electrical conductivities are all too low. Because of low electrical conductivities, their power factors (PF) and figure of merits (ZT) are too low for thermoelectric applications.

Two nano size powder compositions, 0.97 TiO_2 – 0.03 $NbO_{2.5}$ and 1.0 SrO – 1.03x0.8 TiO_2 – 1.03x0.2 $NbO_{2.5}$, were processed and evaluated by a third company. The results show much improved thermoelectric properties. ZTs of 0.25 were seen. Slight composition modification, likely by addition of a highly electrical conductive phase, plus employing SPS sintering technique made the significant improvement of electrical conductivities and therefore power factors and ZTs.

SPS has been identified as a key step for processing high temperature oxide thermoelectric materials.

Particle size reduction of the ceramic thermoelectric composition has benefits. It will be investigated and developed further.

Nb doped $SrTiO_3$ and Nb or Ta doped TiO_2 compositions are good base line compositions for n-type thermoelectric compositions.

No unique p-type thermoelectric compositions were identified in phase I work. $Ca_3Co_4O_9$ currently is the most available p-type thermoelectric composition. Future development of high temperature p-type thermoelectric materials will be needed. It will likely to start with attempting accepter doping of TiO_2 or $SrTiO_3$.

Several $BaTiO_3$ and rare earth titanate based dielectric compositions showed either n-type or p-type behavior with high Seebeck coefficients. Further investigation and development based on these materials is planned in the future.

A preliminary design and optimization of a thermoelectric generator (TEG) that uses the n-type 1.0 SrO – 1.03x0.8 TiO_2 – 1.03x0.2 $NbO_{2.5}$ ceramic thermoelectric material was performed. The optimization design outputs pointed out there is room for improvement of the chosen ceramic material. This modeling and optimization technique is a very useful tool in estimating; (a) how practical physically, technically, and economically to fit chosen thermoelectric materials into an actual module to generate renewed usable energy, (b) optimum design of the TEG device, (c) material consumption of the TEG device, and (d) material and manufacturing cost of the TEG device.

6.0 FUTURE WORKS

Future works are:

Optimize the SrO – TiO_2 – $NbO_{2.5}$, TiO_2 – $NbO_{2.5}$ (or $TaO_{2.5}$), and the dielectric composition systems to improve their thermoelectric properties. Target is to increase ZTs from current value (0.1 - 0.2) to 0.5 or above. Specific technical approaches will be a) to develop an optimum formulation chemistry (dopant level, dopant type, stoichiometry), b) to develop high electrical conductivity additives , c) to develop particle size reduction technology d) to qualify raw material sources for commercialization and e) to develop spark plasma sintering process.

Development and optimization of a non cobaltite based p-type formulation. $SrTiO_3$ and TiO_2 with p-type dopants must be attempted. Composition and process modifications of dielectric formulations are also to be investigated. Technical approaches will be the same as proposed above for n-type materials.

Develop and optimize the SPS process to sinter individual component and module assembly.

Develop oxide conductive materials for the metallization.

Design thermoelectric modules utilizing n-type, p-type, and metallization materials that are developed.

Fabricate prototype module or device and test their performance.

The above planned future work will combine development of ceramic powders and manufacturing expertise at TAM, development of SPS at TAM or a partner organization, and thermoelectric material/module testing, modeling, optimization, production at several partner organizations.

7.0 BIBLIOGRAPHIES

[1] Hendricks, T., et al. "Engineering Scoping Study of Thermoelectric Generator Systems for Industrial Waste Heat Recovery", Industrial Technologies Program, DOE, 2006.

[2] Bass, J. C., et al. "Application of Advanced Thermoelectric Technology to the Diesel Generator", http://www.fischer-tropsch.org/DOE/ conf proc/DEER/970799/conf 970799 pg157.pdf.

[3] LaGrandeur, J., et al., "Automotive Waste Heat Conversion to Electric Power Using Skutterudite, TAGS, PbTe, and BiTe," Proceedings of the 25th International Conference on Thermoelectrics, Vienna, Austria, August 2006.

[4] LaGrandeur, J., "Automotive Waste Heat Conversion to Power Program – 2009 Annual Merit Review", DOE Project ace_47_lagrandeur, May 22, 2009.

[5] Brooks, M. H. (editor), "Thermoelectric Materials", National Lead Company , Titanium Alloy Manufacturing Division, Navy Contract Report NObs 7836, http://handle.dtic.mil/100.2/AD405569.

[6] Kato, K., et al. "The Effect of Eu substitution on thermoelectric properties of $SrTi_{0.8}Nb_{0.2}O_3$", J. Appl. Phys., 102, p116107, 2007.

[7] Ohta, H., "Thermoelectrics based on strontium titanate", Materials toady, V10, No. 10, p44, October, 2007.

[8] Ohta, H., et al. "Critical thickness for giant thermoelectric Seebeck coefficient of 2DEG confined in $SrTiO_3$/ $SrTi_{0.8}Nb_{0.2}O_3$ superlattices", Science Direct, Thin Solid Films 516, p5916, 2008. www.sciencedirect.com.

[9] Tomio, T., et al., "Control of electrical conductivity in laser deposited $SrTiO_3$ thin films with Nb doping", J. Appl. Phys. 76 (10), p5886, November 1994.

[10] Zhao, T., et al., "Highly conductive Nb doped $SrTiO_3$ epitaxial thin films grown by laser molecular beam epitaxy", J. Crystal Growth 212, p451, 2000.

[11] Park, J., et al., "Thermoelectric properties of Bi, Nb co-substituted $CaMnO_3$ at high temperature", J. Alloys and Compounds 487, p550, 2009

[12] Boskovic, S., et al., Nanopowders properties and sintering of $CaMnO_3$ solid solutions", J. Alloys and Compounds 463, p282, 2008.

[13] Melo Jorge, M. E., et al., "Effects of synthesis method on stoichiometry, structure and electrical conductivity of $CaMnO_{3-\delta}$", International Journal of Inorganic Materials 3, p915, 2001.

[14] Xu, G., et al., "High-temperature transport properties of Nb and Ta substituted $CaMnO_3$", Science Direct, Solid State Ionics 171, p147, 2004.

[15] Wang, Y., et al., "Thermal conductivity of electron-doped $CaMnO_3$ perovskites: Local lattice distortions and optical phonon thermal excitation", Acta Mater, doi:10.1016/j.actamat.2010.07.052, 2010.

[16] Yin, T., et al., "Nanocrystalline Thermoelectric $Ca_3Co_4O_9$ Ceramics by Sol-Gel Based Electrospinning and Spark Plasma Sintering", J. Phys. Chem. C2010, p10061, 2010.

[17] Xu, G., et al., " Thermoelectric properties of Bi- and Na- substituted $Ca_3Co_4O_9$ system", Applied Physics Letters, V80, No. 20, p3760, 2002.

[18] Funahashi, R., et al., "Thermoelectric properties of $Bi_2Sr_2Co_2O_x$ polycrystalline materials", Applied Physics Letters, V76, No. 17, p2385, 2000.

[19] Masset, A. C. et al., "Misfit-layered cobaltite with an anisotropic giant magnetoresistance: $Ca_3Co_4O_9$", Physical Review B, V62, No. 1, p166, 2000.

[20] Xu, L., et al., " High-temperature transport and thermoelectric properties of $Ca_3Co_{4-x}Ti_xO_9$", J. Alloys and Compounds 501, p115, 2010.

[21] Wei, B., et al., "Crystal structure, thermal expansion and electrical conductivity of perovskite oxides $Ba_xSr_{1-x}Co_{0.8}Fe_{0.2}O_{3-\delta}$ ($0.3 =< x =< 0.7$), Science Direct, J. European Ceramic Society 26, p2827, 2006.

[22] Li, S., et al., "Performance of $Ba_{0.5}Sr_{0.5}Co_{0.6}Fe_{0.4}O_{3-\delta}$–$Ce_{0.8}Sm_{0.2}O_{1.9}$ composite cathode materials for IT-SOFC", J. Alloys and Compounds 448, p116, 2008.

[23] Chaim, R., "Densification mechanisms in spark plasma sintering of nanocrystalline ceramics", Materials Science Engineering A443, p25, 2007.

[24] Belmonte, M., "Spark plasma sintering: A powerful tool to develop new silicon nitride-based materials", Science Direct, J. of the European Ceramic Society 30, p2937, 2010.

[25] Orru, R., "Consolidation/synthesis of materials by electric current activated/assisted sintering", Materials Science and Engineering R, 63, p127, 2009.

[26] Aalund, R., " Unveiling Spark Plasma Sintering High-Throughput Processing", www.thermaltechnology.com

8.0 LIST OF TABLES

Table **Page**

9.0 LIST OF FIGURES

Figure **Page**

Figure **Page**

10.0 LIST OF ACRONYMS AND ABBREVIATIONS

Ar	Argon Gas
CHX	Coolant Heat Exchanger
DC	Direct Current
DOE	Department of Energy
DTA	Differential Thermal Analysis
EHX	Exhaust Heat Exchanger
EIA	Electronic Industry Association
H2	Hydrogen Gas
ICP	Induction Coupled Plasma
KWH	Kilo Watt Hour
LN	Natural Logarithm
LOI	Loss on Ignition
NASA	National Aeronautics Space Administration
NDA	Non Disclosure Agreement
SEM	Scanning Electron Microscope
SPS	Spark Plasma Sintering
TE	Thermoelectric
TEG	Thermal Electric Generator
TGA	Thermogravimetric Analysis
XRD	X-Ray Diffraction
X7R302H	Commercial dielectric powder with high sintering temperature (> 1200°C, H), has dielectric constant of 3000 (302), meets EIA X7R temperature coefficient specification
NPO610H	Commercial dielectric powder with high sintering temperature (> 1200°C, H), has dielectric constant of 61 (610), meets EIA NPO temperature coefficient specification
Y5V153L	Commercial dielectric powder with low sintering temperature (< 1200°C, H), has dielectric constant of 15,000 (153), meets EIA Y5V temperature coefficient specification

Z5U113H	Commercial dielectric powder with high sintering temperature (> 1200°C, H), has dielectric constant of 11,000 (113), meets EIA Z5U temperature coefficient specification
X7R	EIA temperature coefficient specification for dielectric material (dielectric constant change of less than +/- 15% from -55°C to 125°C reference to 25°C)
NPO	EIA temperature coefficient specification for dielectric material (dielectric constant change reference to dielectric constant at 25°C of less than +/- $30x10^{-6}$/°C from -55°C to 125°C reference to 25°C)
Y5V	EIA temperature coefficient specification for dielectric material (dielectric constant change of less than +22% and less than < -56% from -30°C to 85°C reference to 25°C)
Z5U	EIA temperature coefficient specification for dielectric material (dielectric constant change of less than +22% and less than -56% from 10°C to 85°C reference to 25°C)
PF	Power Factor, Unit = Watt/m-K^2
psi	Pressure per Square Inch, Unit = lb/inch^2
Q	Seebeck Coefficient, Unit = μV/K
σ	Electrical Conductivity, Unit = S/cm
k	Thermal Conductivity, Unit = Watt/m-K
T	Temperature, Unit = C or F or K
C	Temperature as Centigrade
F	Temperature as Fahrenheit
K	Temperature as Kelvin
W	Watt
Watt	Unit of Power
ZT	Figure of Merit, Unit = Dimensionless
μ	Micro (10^{-6})
nm	Unit of Length as 10^{-9} meter
μm	Unit of Length as 10^{-6} meter
mm	Unit of Length as 10^{-3} meter
cm	Unit of Length as 10^{-2} meter

m	Unit of Length as meter